

Bates College

SCARAB

Standard Theses

Student Scholarship

5-2020

Exploring the Possibility of Liquid Immiscibility in the Ste. Dorothée Sill near Montréal, Québec

Michael Cooper
mcooper@bates.edu

Follow this and additional works at: https://scarab.bates.edu/geology_theses

Recommended Citation

Cooper, Michael, "Exploring the Possibility of Liquid Immiscibility in the Ste. Dorothée Sill near Montréal, Québec" (2020). *Standard Theses*. 46.
https://scarab.bates.edu/geology_theses/46

This Open Access is brought to you for free and open access by the Student Scholarship at SCARAB. It has been accepted for inclusion in Standard Theses by an authorized administrator of SCARAB. For more information, please contact batesscarab@bates.edu.

Exploring the Possibility of Liquid Immiscibility in the Ste. Dorothée Sill near Montréal, Québec

A Senior Thesis
Presented to
The Faculty of the Department of Geology
Bates College



In partial fulfillment of the requirements for the
Degree of Bachelor of Science

Michael Gehn Cooper

Lewiston, Maine
April 9th, 2019

ACKNOWLEDGEMENTS

I would first like to thank my parents for providing me with all of the wonderful opportunities I've had the pleasure of experiencing throughout my life. Both of you are my inspiration in life. I have watched you work tirelessly to provide Faith and I with the kind of support I can only hope to provide my own children one day. Because of that support, I am at Bates College, having written an undergraduate thesis I am incredibly proud of. Without you, this could have never been an opportunity for me.

I would also like to thank Dr. Geneviève Robert. Without your help and guidance throughout this year, I would certainly not have a project that I am proud of. You helped with revisions constantly and helped me understand difficult topics that I had no experience with. Definitely the best advisor I could have hoped for!

Thank you to the Geology Department for being a place I enjoy being a part of. Everyone in the Geology Department, including the students, are amazing individuals and have all added to my wonderful Bates experience thus far.

Finally, I would like to thank the Ski Team and all of my other friends at Bates. You've given me distractions that kept me sane throughout this entire process, which I really appreciate. I certainly could not have had as much fun throughout this year if it wasn't for all of you.

ABSTRACT

Philpotts (1972) suggests the presence of an immiscible liquid (ocelli) crystallized within the Sté Dorothée Sill near Montréal, Canada. To test this hypothesis, I use the alphaMELTS program (Antoshechkina et al., 2012) which combines thermodynamic data and bulk compositional data to mimic natural magmas as they crystallize in the crust. Isobaric and isentropic models are used to simulate both the emplacement conditions and the source conditions of the parent magma that formed the Sté Dorothée Sill. The isobaric model uses temperature constraints that are unrealistic for emplacement, however ensure the composition is entirely liquid upon emplacement in order to compare the modal mineralogy of the sill. The mineral groups that crystallize from the isobaric trials are largely similar to the mineral groups observed in the Sté Dorothée Sill. Isentropic trials present a more realistic representation of the sill's emplacement. Upon ascent from 1 GPa to 300 bars, the mineralogy of the crystallized portion of the melt in both trials suggest a mineralogy similar to the host fourchite which surrounds the ocelli. The remaining liquid upon reaching the suggested emplacement depth closely resembles the chemical composition of the hypothesized immiscible liquid. This evidence suggests that the liquid, which was previously thought to be of immiscible origin, was instead the result of fractional crystallization.

TABLE OF CONTENTS

Table of Figures	vi
Table of Tables	vii
Introduction	8
1.1 Alkaline Rock Genesis and Nomenclature	8
1.2 Tectonic Settings of Igneous Rocks	13
1.3 Liquid Immiscibility	14
1.4 Monteregean Igneous Province	17
1.5 Ste. Dorothée Sill	19
1.6 Description of Ocelli within the Ste. Dorothée Sill	20
1.7 Hypotheses for the Origin of Ocelli and Felsic Units	23
2 METHODS	26
2.1 Overview	26
2.2 Volume Calculations for Ocelli	26
2.3 Calculations for Felsic Units	28
3 MODELING	32
3.1 Background of the alphaMelts Program	32
3.2 Isobaric Experimental Trials	33
<i>3.2.1 Parental Liquid Composition</i>	<i>33</i>
3.3 Isentropic Experimental Trials	35
4 RESULTS	37
4.1 Crystallization in the Upper Crust	37
<i>4.1.1 Modal Mineralogy</i>	<i>38</i>
4.2 Melt Ascent from Source Region	42
<i>4.2.1 Crystallization of Remaining Liquid from Isentropic Trials</i>	<i>43</i>
5 DISCUSSION	48
5.1 Liquid Immiscibility in Alkaline Magmas	48
5.2 Effectiveness of alphaMELTS for Modeling Liquid Immiscibility	49
5.3 Isobaric Interpretations	49
<i>5.3.1 Mineral Interpretations</i>	<i>50</i>
5.4 Isentropic Interpretation	52
<i>5.4.1 Remaining Liquid after Adiabatic Ascent</i>	<i>53</i>
<i>5.4.2 Crystallization of the Remaining Liquid After Adiabatic Ascent</i>	<i>55</i>
5.5 Significance of the Carbonate Liquids and the Oka Intrusion	55

5.6 Future Work	57
6 CONCLUSION	59
References	61
Appendix A: Equations	64
Appendix B: Melts Files	65

TABLE OF FIGURES

Figure 1.1 Alkali-Silica Plot	9
Figure 1.2 Olivine-Nepheline-Quartz Ternary Diagram.....	10
Figure 1.3 AFM Ternary of Subalkaline Rocks.....	11
Figure 1.4 An-Ab-Or Ternary of Sodic and Potassic Rocks.....	11
Figure 1.5 Normative Color Index of Plagioclase	12
Figure 1.6 Fayalite-Leucite-Silica Ternary	15
Figure 1.7 Immiscible Liquids in Hawaiian Basalts	16
Figure 1.8 Map of the Montereian Igneous Province	18
Figure 1.9 Cross-section of the Sté Dorothée Sill.....	21
Figure 1.10 Graph of Ocelli Density in Sté Dorothée Sill	22
Figure 2.1 Image of Felsic Layer 2	29
Figure 2.2 Image of Felsic Layer 3	30
Figure 3.1 Representation of the Isentropic Model.....	36
Figure 4.1 Mineral and Liquid Proportions of Isobaric Model.....	38
Figure 4.2 Immiscible Liquids from Isobaric Model.....	41
Figure 4.3 Minerals in MC2 Remaining Melt.....	46
Figure 4.4 Minerals in MC10 Remaining Melt.....	46
Figure 4.5 Immiscible Liquids from Isentropic Model.....	47
Figure 5.1 Rayleigh-Taylor Instability	54
Figure 5.2 Oka Pluton	56

TABLE OF TABLES

Table 2.1 Calculations of Ocelli by Layer	28
Table 3.1 Bulk Compositions of Ocelli by Volume.....	34
Table 4.1 Isobaric Crystallization of Trials MC2 and MC10	39
Table 4.2 Minerals in MC2 Ascent from 1 GPa	42
Table 4.3 Minerals in MC10 Ascent from 1GPa	42
Table 4.4 Bulk Composition of Remaining Liquids	44,53
Table 4.5 Isobaric Crystallization of Remaining Liquids	45

INTRODUCTION

In this thesis, I use petrological modeling to test the hypothesis of liquid immiscibility in the Ste. Dorotheé sill, largely composed of a groundmass of silica-rich fourchite. Philpotts (1972) proposed liquid immiscibility as the mechanism that produced the two separate fourchite type units found in the sill. Liquid immiscibility corresponds to the separation of a homogenous magma into two or more liquids. Liquid immiscibility is one of many different mechanisms that offer explanations for the differentiation of magmas. Liquid immiscibility has been observed in tectonic rifting zones and in magmas from hotpots. Focusing on the Ste. Dorotheé Sill, I conducted research that uses bulk rock compositional data of the sill to test whether Philpotts' hypothesis of liquid immiscibility is responsible for the compositional differences seen throughout the sill.

1.1 Alkaline Rock Genesis and Nomenclature

Joseph Iddings first proposed the idea that igneous rocks fall into specific categories or series based upon parent magmas of silicic types in the late 1800s. His proposal included that all igneous rocks fell into two categories; subalkaline series and alkaline series. The distinctions between the two series could initially be conducted in the field based upon both mineralogical characteristics and tectonic setting (Winter, 2010). By using microscopic techniques, Iddings was able to identify slight mineralogical differences between igneous rocks to develop a complex classification involving geographical location and mineralogical differences. He defined augite as the most prevalent mineral found in igneous rocks, which due to its variability in color, can be used to differentiate igneous rocks based upon location. Iddings also noted other minerals such as quartz, orthoclase-feldspar, and biotite to classify igneous rocks based on location (Iddings, 1892). In 1909, Alfred Harker characterized the series further from the geographical attributes

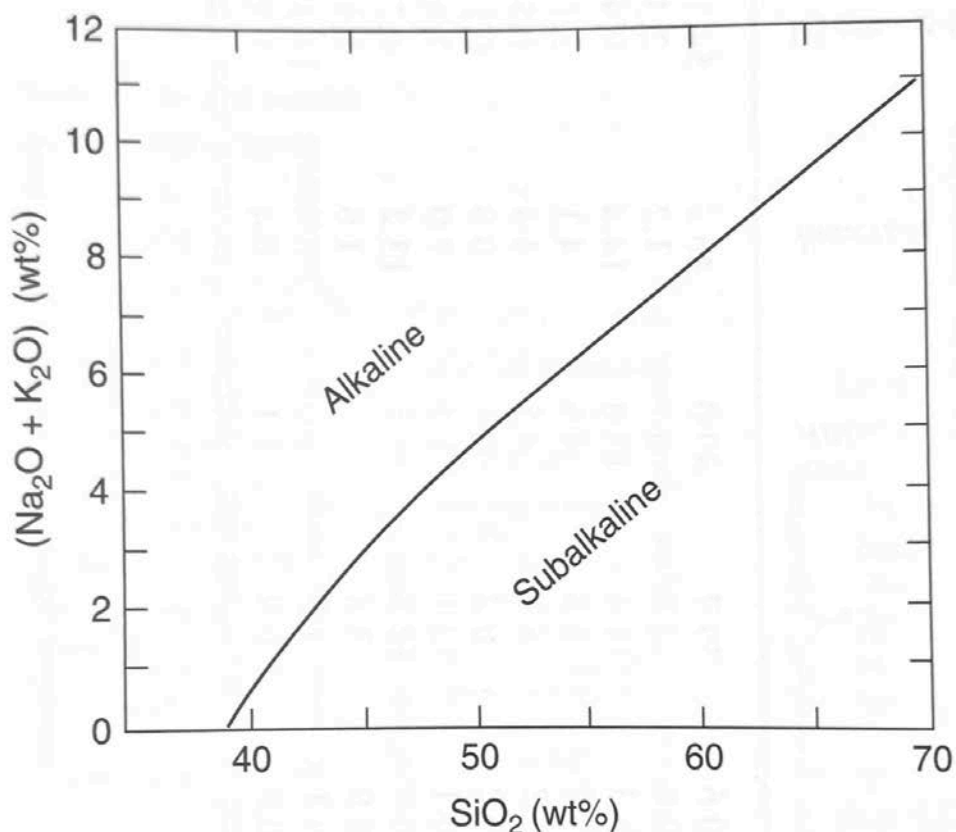


Figure 1.1: Alkali-Silica plot distinguishing the boundary between alkaline rocks and subalkaline rocks. This line was derived from an equation created by Irvine and Baragar (1971). The equation for the line defined by Irvine and Baragar can be found in Appendix A (Philpotts and Ague, 2009)

proposed by Iddings. By using this classification, Harker was able to identify Cenozoic volcanic activity and used this to see differences between igneous rocks found in the Pacific and Atlantic oceans. Harker suggested that alkaline rocks bordered the Atlantic Ocean whereas subalkaline rocks bordered the Pacific. Further research and classification conducted by Irvine and Baragar (1971) helped them redefine the two series and added peralkaline as an addition to Iddings' proposed series (Philpotts and Ague, 2009). Irvine's and Baragar's classification of igneous rocks is the most modern and widely accepted to date.

The division of the three main groups is based upon the alkali content of the rocks. Alkaline rocks are alkali rich and are usually undersaturated with silica, whereas subalkaline rocks are silica saturated to silica oversaturated (Winter, 2010). Silica saturation pertains to the amount of silica-based minerals in the rock. If a magma is oversaturated with silica, quartz will

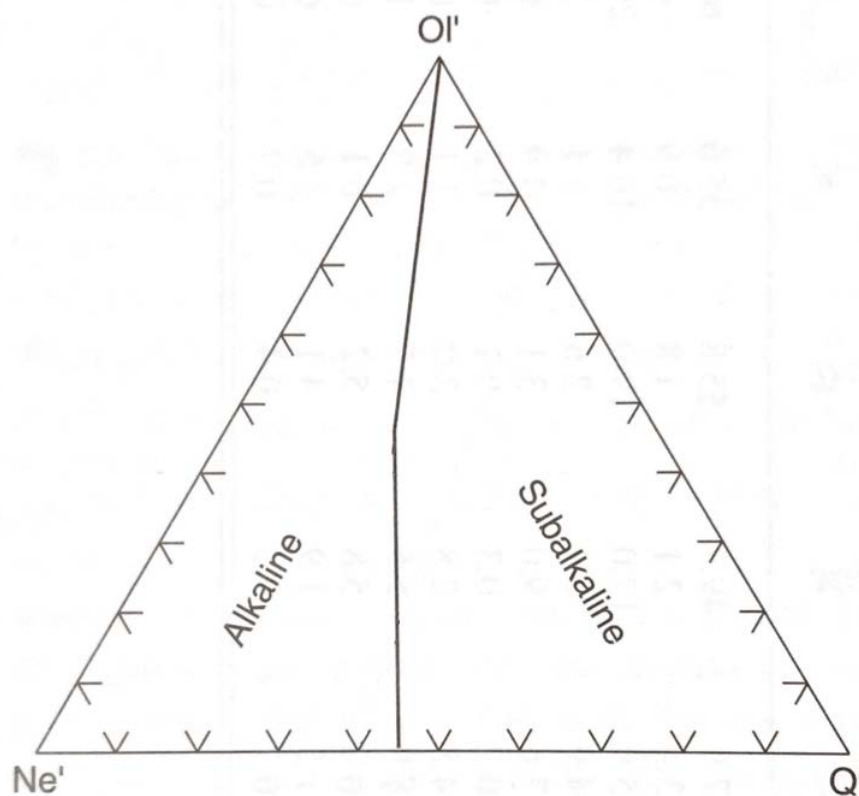


Figure 1.2: Olivine-Nepheline-Quartz ternary plot distinguishing alkaline and subalkaline rocks. This plot is based upon the percent of cation equivalents (represented by the ' symbol) found in the rock. Equations for each of the corners are provided in Appendix A that calculate the composition of (cation) normative minerals. The solid line represents the division between subalkaline and alkaline rocks (Philpotts and Ague, 2009).

precipitate out of the magma and be present in the cooled rock. If a rock is undersaturated with respect to silica, quartz will not precipitate out of the magma and will not appear in the crystallized rock. Peralkaline rocks are alkali rich like the previous two series, however they are defined with respect to their Al_2O_3 concentrations and will not be as important to the discussion of this thesis. The distinction between subalkaline and alkaline rocks is calculated through an equation created by Irvine and Baragar based upon the total $Na_2O + K_2O$ weight percentage versus the silica weight percent (Irvine and Baragar, 1971). This equation can be seen in Appendix A. Figure 1.2 shows the alkali-silica plot with the line distinguishing the boundary between alkaline and subalkaline. These groups can also be represented in a modal mineralogy diagram based on olivine, nepheline, and quartz, which uses an equation that can be found in

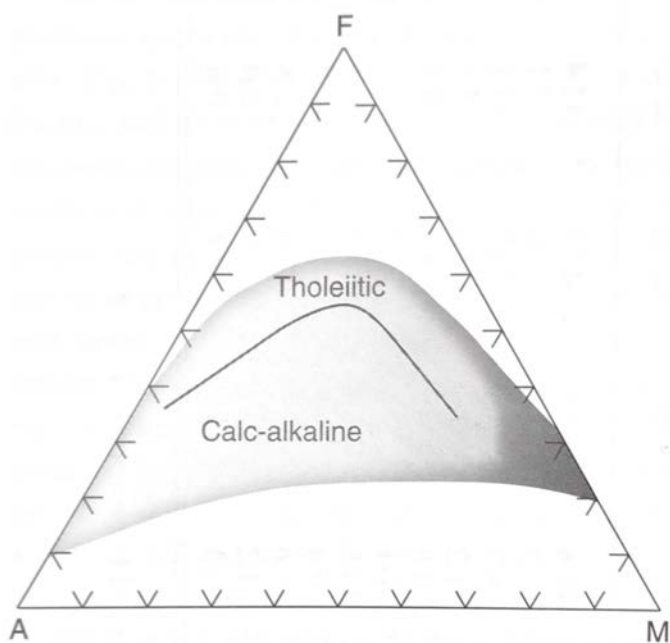


Figure 1.3: Irvine and Baragar's (1971) AFM plot classifying the subalkaline series into tholeiitic and calcalkaline rocks based upon weight percentages. A; $\text{Na}_2\text{O} + \text{K}_2\text{O}$. F; $\text{FeO} + 0.8998\text{Fe}_2\text{O}_3$. M; MgO . The boundary line between tholeiitic and calc-alkaline is not defined completely across the plot since the distinction between rocks becomes difficult on the mafic and felsic ends of the plot (Philpotts and Ague, 2009).

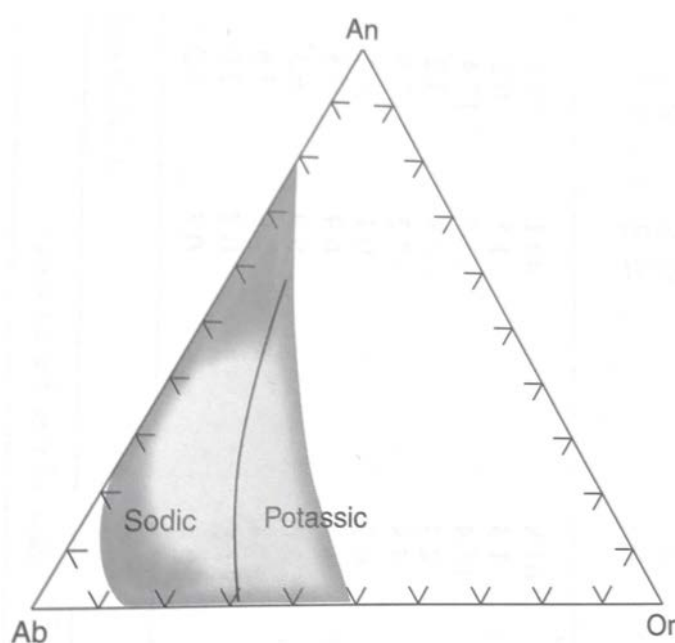


Figure 1.4: An-Ab-Or plots distinguishing the boundary between sodic and potassic series based upon percent cation equivalents. The equation governing the defined line can be found in Appendix A. These series belong to the main alkali olivine basalt series (Irvine and Baragar, 1971).

Appendix A. In Figure 1.2, alkaline rocks are plotted on the nepheline side of the diagram whereas subalkaline rocks are plotted on the quartz side (Philpotts and Ague, 2009).

The subalkaline series is further subdivided into the tholeiitic series and the calcalkaline series as represented in Figure 1.3. This figure shows this distinction between subalkaline and calcalkaline rocks which is based upon their iron content. As the rocks become more mafic or felsic, there is overlap between the two series. When the rocks are considerably felsic, there is no way to distinguish between calcalkalic and tholeiitic members, therefore all granitic rocks are assigned to the calcalkalic series. According to Irvine and Baragar (1971), these can also be further distinguished by plotting the Al_2O_3 weight percentage versus the normative plagioclase. Calcalkaline basalts and andesites contain roughly 16%-20% Al_2O_3 , which is shown when they are plotted on an AFM (alkali oxides $\text{Na}_2\text{O} + \text{K}_2\text{O}$, iron oxide $\text{FeO} + \text{Fe}_2\text{O}_2$, and magnesium

oxide MgO diagram). Theoleiitic rocks contain less Al_2O_3 , whereas calc-alkaline rocks generally consist of 12%-16% Al_2O_3 (Philpotts and Ague, 2009).

The alkaline series is further subdivided into the alkaline olivine basalt series and the nephelinitic-leucite-analcite series (Philpotts and Ague, 2009). The alkali olivine basalt series is defined on the basis of its normative feldspar composition (Philpotts and Ague, 2009). There are two subseries of rock that are associated with the alkali olivine basalts: the sodic series and the potassic series. The boundary between sodic and potassic rocks are defined by their K_2O/Na_2O ratio (Mitchell, 1996). Potassic rocks contain a larger percentage of K_2O , while sodic rocks contain more Na_2O (Winter, 2010). Figure 1.4 shows Irvine and Baragar's (1971) classification based upon the normative albite-anorthite-orthoclase within the rock represented through their cation equivalents. Many of the alkaline series have color indices which help to further define

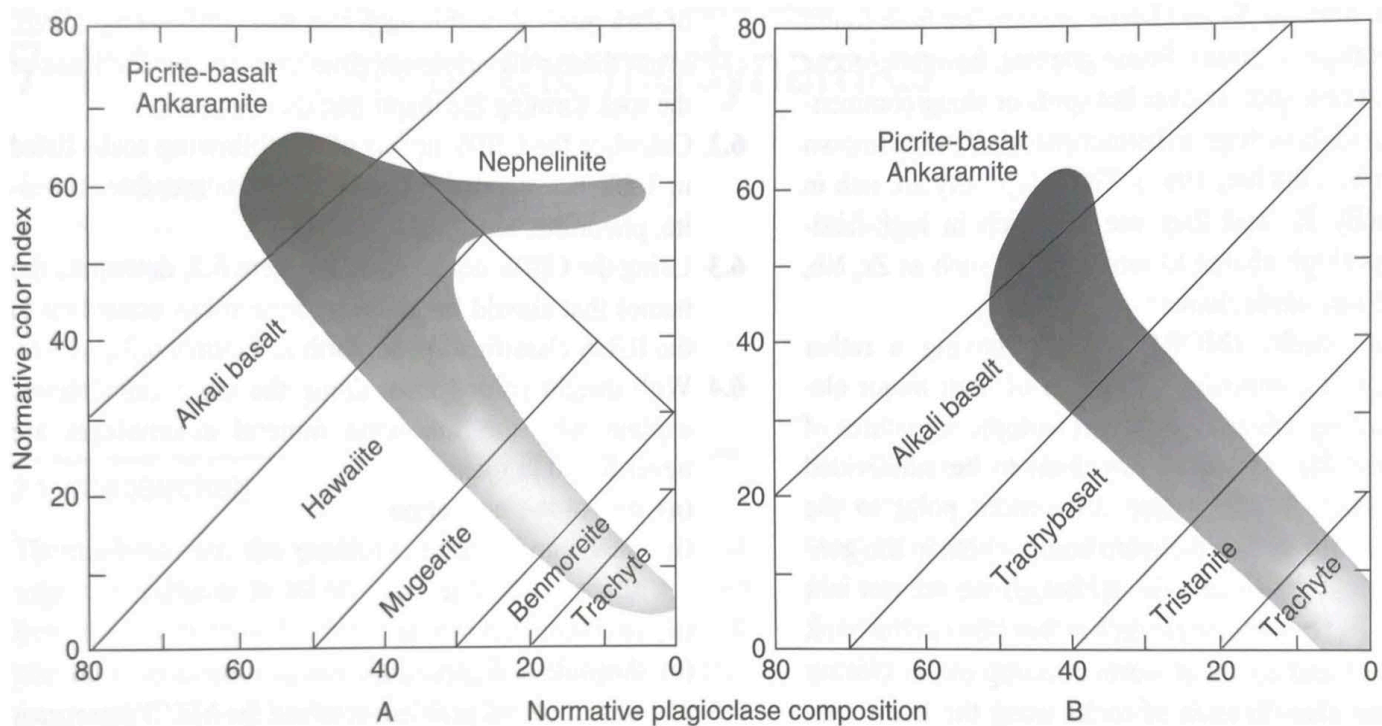


Figure 1.5: Plots of the normative color index versus normative plagioclase composition. (A) Sodic series (B) Potassic series. The equations that govern the boundary lines can be found in Appendix A (Irvine and Baragar, 1971). Images of these plots were provided by Philpotts and Ague (2009).

and recognize differences in these igneous rock series. Figure 1.5 shows further distinction between the two subseries and the rocks that exist within them. Both of these subseries contain mafic derivatives called alkali picrite-basalt and ankaramite, however these derivatives are difficult to distinguish due to the low concentration of alkalis in the rocks (Irvine and Baragar, 1971). Rocks within the nephelinitic-leucite-analcite series typically contain less than 45% SiO_2 and have color indices greater than 50, and in some cases they contain small amounts of leucite (Philpotts and Ague, 2009). Even though the use of the color index is a qualitative description, it is useful in telling the difference between dark colored (mafic) and light colored (felsic) minerals. The values shown on the y-axis in Figure 1.5 show the ratio between mafic and felsic rocks. Using the combination of these features, the nephelinitic-leucite-analcite series can be easily distinguished from the alkali olivine basalt series.

The alkaline, tholeiitic, and calc-alkaline rock series are the most dominant series and represent a large part of the igneous history of the Earth. Based upon the chemical composition, geologic setting can be derived from alkaline rocks that further describe tectonic activity such as orogenic belts, subduction zones, crustal extension, mid-ocean ridges, and continental rifting (Philpotts and Ague, 2009).

1.2 Tectonic Settings of Igneous Rocks

The largest volumes of alkaline rocks are associated with continental rift systems. During early stage rifting and rift systems, flood basalts are common and produce almost entirely alkaline rocks. Many continental rift magmas have a similar composition to that of oceanic intraplate basalts (Allègre et al., 1981). Oceanic intraplate basalts are thought to have formed from deep mantle plumes, which suggests the contribution of the lower mantle to the production of alkaline magmas in continental rift systems (Haase and Renno, 2008). The Mesozoic Era produced many

alkaline rocks, specifically along failed branches of rifting zones during the breakup of Pangaea (Philpotts and Ague, 2009). The process in which rift zones produce alkaline magma flows is highly debated in the scientific community. Some researchers suggest that asthenospheric upwelling forces the lithosphere to spread apart, making way for new magma to push through and create new rock. However, other researchers suggest that the mechanism of plate spreading causes weakness and collapse in the lithosphere which allows the asthenosphere to rise and fill in the space created (Winter, 2010).

Bodies of igneous rocks are divided into plutonic, hypabyssal, and volcanic depending on their depth of emplacement. There is no definitive separation between hypabyssal and plutonic, however grain size is the distinction many petrologists use. Volcanic and hypabyssal rocks form on or near the surface of the Earth. Volcanic rocks were classified by Irvine and Baragar (1971) and provided geographical and formation characteristics for each of the igneous series. The calc-alkali series discussed in the previous section is characteristic of volcanic island arcs and orogenic belts which is indicative of subduction zones. Tholeiitic rocks are developed in areas of crustal extension and in areas characterized by flood basalts (Philpotts and Ague, 2009). Many alkali olivine basalts and similar alkali rocks are associated with areas of continental rifting or in regions overlying deeply subducted plates (Philpotts and Ague, 2009).

1.3 Liquid Immiscibility

Liquid immiscibility corresponds to the separation of one magma into two or more, compositionally unique magmas. The idea behind liquid immiscibility had been considered as early as the beginning of the 20th century, however petrologists struggled to find evidence that strongly supported immiscibility in magmas (Bowen, 1928). Bowen suggested that immiscibility is a phenomenon that occurs in a natural magma that separates into basalt and rhyolite, however

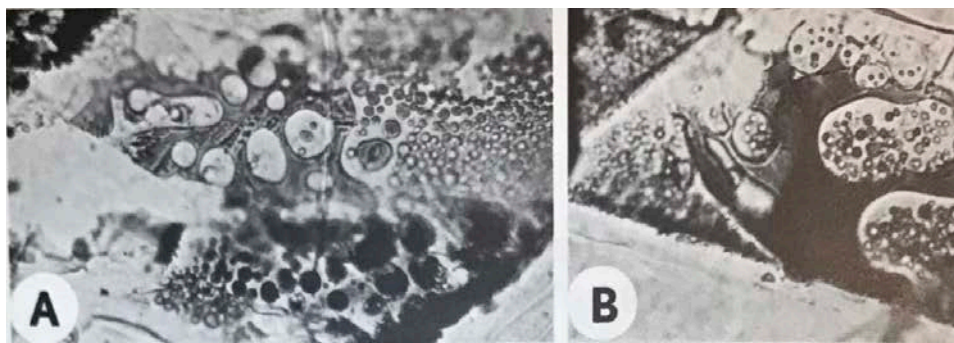


Figure 1.7: (A) Globules of an immiscible liquid are seen to exist within one another in a tholeiite glass from Kilauea, Hawaii. (B) Smaller globules seen in an olivine-basalt sample from Mauna Loa, Hawaii (Philpotts, 1982)

sample, there must be two chemically unique glasses preserved within one another in the form of globules (Philpotts, 1982). Examples of the globule structures are seen in Figure 1.7 in two separate magmas from Hawaii. Many studies have been conducted focusing on tholeiitic magmas and the compositional changes that occur upon their crystallization. Charlier and Grove (2012) found that as tholeiitic magmas cool, silicate liquid immiscibility is common. As minerals crystallize out of the magma, the proportion of alkalis, phosphorous, and titanium in the remaining melt increases, leading to the development of two separate liquids. This produces one mafic liquid and one more evolved liquid (Charlier and Grove, 2012). Low-pressure fractional crystallization in these systems is the most favorable condition that produces the unmixing of liquids.

Alkaline systems, which are the focus of this thesis, behave differently than tholeiitic systems upon crystallization. Liquid immiscibility in tholeiitic basalts is quite common, whereas it is rare in alkaline magmas (Philpotts, 1982; Philpotts and Ague, 2009). Alkaline magmas contain higher proportions of oxides that are known to expand the field of immiscibility in tholeiitic basalts. Oxides such as titanium, phosphorous, and iron can be critical to the development of immiscible liquids (Freestone, 1978; Visser and Groos, 1979). Despite being chemically similar, the larger proportion of alkalis in alkaline rocks significantly changes the

way alkaline magmas crystallize compared to tholeiitic magmas. One would assume the presence of more alkalis would suggest a larger number of examples of liquid immiscibility in alkaline magmas, however only a limited number have been successfully studied (Freestone, 1978; Philpotts, 1982; Philpotts and Hodgson, 1968).

The few examples of alkaline liquid separation are important to explain features in many alkalic dikes in the Montereian Igneous Province in Canada, even though their chemical compositions vary slightly. The alkaline magmas are thought to produce small, globular structures called ocelli which can coalesce to form larger bodies of a separate, more felsic composition.

1.4 Montereian Igneous Province

Continental rifting is known to produce alkaline magmas (Allègre et al., 1981; Haase and Renno, 2008; Sengör and Burke, 1978), which is consistent with alkaline intrusions in the Montereian Igneous Province. The rifting of Pangaea is the broader tectonic process that preceded the formation of these intrusions. However, the regional tectonic process that formed the intrusions in the Montereian Igneous Province (MIP) has been highly debated by geologists since the early 1980s. Crough (1981) hypothesized that the passing of the North American plate over a mantle hotspot, called the Great Meteor Hotspot in the deep mantle, was the source of these intrusions. The intrusions extend from the oldest intrusions in southeastern Canada, through the White Mountains in New Hampshire, all the way to the younger New England seamounts in the Atlantic ocean (Crough, 1981). Studies after Crough (1981) dispute his hypothesis suggesting the Great Meteor Hotspot is not responsible for all of the intrusions expanding across the region.

Eby and McHone (1997) suggest the MIP can be divided into two episodes of intrusive activity, one during the Jurassic (170-200 Ma) and one during the Cretaceous (125 Ma). Instead of following the Great Meteor Hotpost track, the age of the intrusions seen in the White Mountains of New Hampshire are older than those in MIP (Eby and McHone, 1997). In an earlier paper, McHone (1996) discusses that the New England seamounts to the southeast are at least 20 million years too young for the intrusions found in New England, further discrediting the Great Meteor Hotspot hypothesis. Eby (1985) found contrasting results by looking at Sr and Pb isotope ratios in rocks from the MIP and New England seamounts. The isotopic ratios suggested that the Great Meteor Hotspot only provided heat energy that melted the sub-lithospheric mantle source, rather than the deep mantle source (Eby, 1985). In the same paper however, Eby (1985)

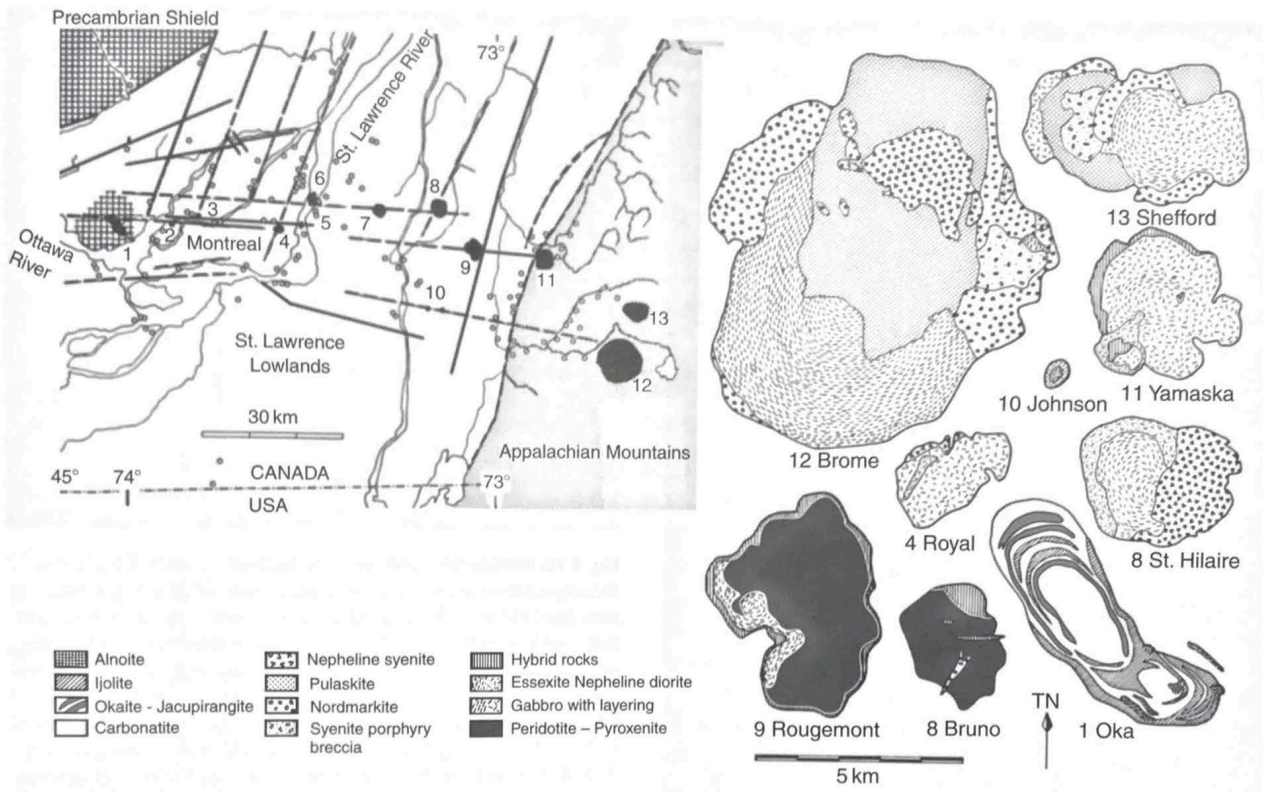


Figure 1.8: This figure represents the Cretaceous Monteregian intrusions of southern Quebec. This linear belt extends eastward from the Ottawa graben across the St. Lawrence Lowlands into the Appalachian Mountains. For the purpose of this thesis, the most important intrusion is the Ste. Dorothée intrusion is labeled number 3 in this figure (Philpotts and Ague, 2009).

used a different method that compared Pb radiogenic isotope composition of the New England seamounts that indicated a direct contribution of the deep mantle material from the Great Meteor Hotspot.

Despite the debated timeline of all the intrusions from the MIP to the New England seamounts, the chemical compositions of the intrusions are consistent among studies in the MIP. The intrusions in the MIP can be seen in Figure 1.8. Silica concentrations in the rocks vary with distance along the east-west faults in the MIP described by Philpotts and Hodgson (1968). The silica content of the rock increases eastward, which may correlate to the thickening of the crust in that direction. The increase in crustal thickness may account for contamination of silica and provide the reason for compositional differences in the dikes and sills seen throughout the MIP (Philpotts and Ague, 2009). East of the St. Lawrence Lowlands, the plutons become larger and the rock in the region become silica saturated to silica oversaturated (Eby and McHone, 1997). The only reason for the slight chemical differences was contamination of the magma coming up through a thicker crust. Philpotts (1970) classifies the Monteregeian intrusions into two groups. One of the groups range from peridotite to gabbro and the other group is classified as syenitic.

1.5 Ste. Dorothée Sill

The Ste. Dorothée Sill is just west of the island of Montreal, sitting between the Mount Royal and Oka plutons and was first described by Howard et al. in 1922. There are seven sill-like bodies in the area, all composed of fourchite suggesting that they originated from the same source (Lentz et al. 2006). Fourchite is a hypabyssal rock that is related to the nepheline syenite. Dikes and sills are rare in western Quebec, however the sills that all chemically correspond with the Ste. Dorothée sill are found closest to the Mont Royal intrusion. These fourchite sills almost

completely lack feldspar (Clark, 1972). A chemically identical sill to the Ste. Dorothée sill is found to the southwest near a town called Ste. Rose.

The Ste Dorothée sill was main sill was best exposed in a quarry which has since been filled. Before the quarry was filled, Philpotts was able to describe the sill in detail. It has a thickness of 5.45 meters and intrudes the Lower Ordovician Beekmantown dolomite. (Philpotts, 1972). Philpotts (1972) suggests that the rock in the Ste. Dorotheé sill is that of analcite syenite, which is the groundmass within what is defined as fourchite. Phenocrysts of titanaugite and hastingsite amphibole are a large component of the sill, estimated to constitute roughly 10% of the sill's volume (Philpotts, 1972). The composition of the groundmass includes hastingsite, titanaugite, magnetite, and an aggregate of analcite, plagioclase, and alkali feldspar (Philpotts and Hodgson, 1968). Included within the sill are rounded feldspathic material called ocelli. Philpott's uses these ocelli as an argument for the presence of an immiscible phase within the sill.

1.6 Description of Ocelli within the Ste. Dorothée Sill

Philpotts (1972) defines the ocelli as small, rounded feldspathic material largely composed of alkali feldspar, analcite or quartz, some even including minor amounts of hornblende or pyroxene (Philpotts, 1972). Philpotts has strategically focused on the sill near Ste. Dorothée, as the ocelli within this sill were better exposed than the other sills in the Monteregian Hills igneous province. The ocelli mapped by Philpotts range in diameter from less than 1 mm to 5 cm and are largely concentrated in the chilled margins of the sill. Other structures labeled as felsic units occur as layers in the upper part of the sill and have the same chemical composition as the ocelli. In this thesis, I test Philpotts' hypothesis of liquid immiscibility as the origin of

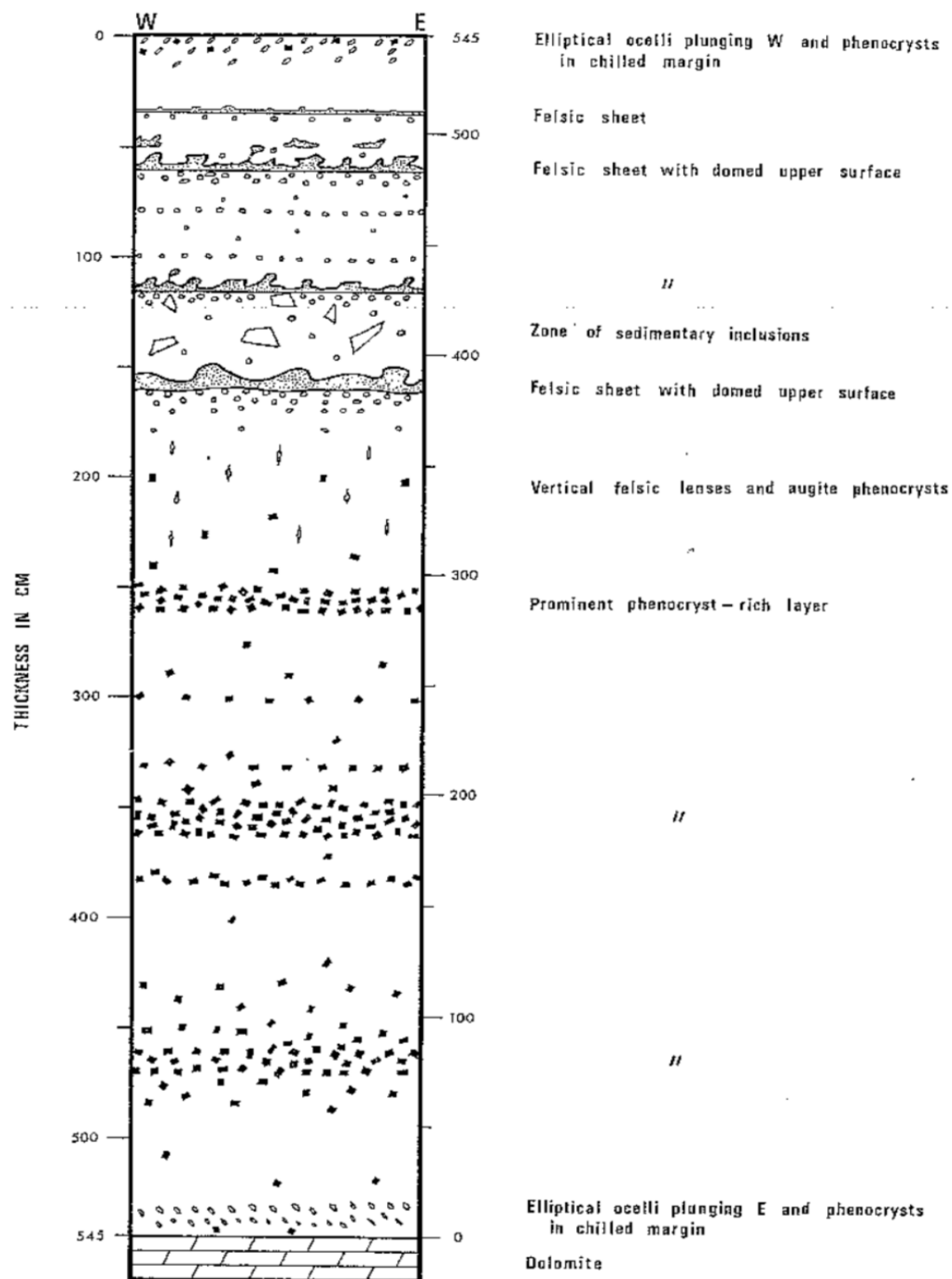


Figure 1.9: Cross-section of the Ste. Dorothée sill provided by Philpotts (1972) with brief indications of the main places where ocelli and felsic units are present. This diagram is not drawn to scale. (Philpotts, 1972)

ocelli in the Ste. Dorothée sill, thus the following descriptions will be entirely from his 1972 paper. A cross-section outlining the sill according to Philpotts (1972) is provided in Figure 1.9.

Starting from the bottom contact of the sill, the ocelli are extremely small but frequent in number. Moving from the lower chilled contact up to 12 cm, the ocelli become larger in size and less frequent, reaching a maximum diameter of 1 mm. The ocelli in this section is outlined in Figure 1.10. The ocelli then disappear at 15 cm from the bottom and do not reappear until 360 cm above the bottom chilled margin. At this point, the ocelli increase in abundance until the 375 cm above the bottom and are all roughly 5mm in diameter. Between 375 cm and 445 cm, the abundance of ocelli relative to the host is not reported, but ocelli exists within a matrix of the host fourchite and sub-angular xenoliths of dolomite and feldspathic sandstone. There are two slightly concentrated layers of ocelli roughly 5 mm in diameter at 445 cm and 467 cm from the bottom contact. From 467 cm to 485 cm, ocelli increase in abundance and again, have diameters around 5mm. The felsic lenses at this layer have flat bases and diapiric structures that rise 1 to 2

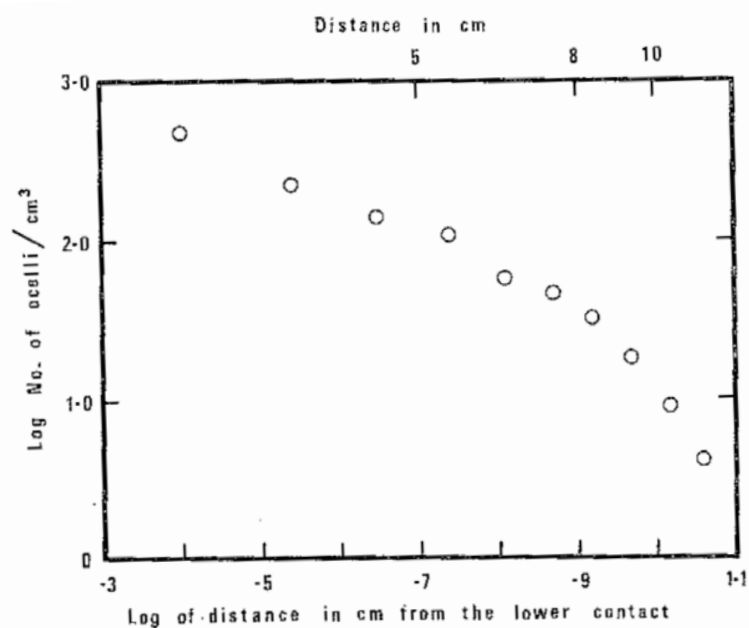


Figure 1.10: Plot of the logarithm of the number of ocelli per cm^3 versus the logarithm of the distance from the lower contact of the sill (Philpotts, 1972).

cm above the flat bases. Above this layer, ocelli are present with a diameter of 3 mm until 512 cm and increase in frequency until 530 cm above the base. At this point, the upper chilled margin contains ocelli that vary in size less than 2 cm decreasing towards the upper contact mimicking the trend observed in the lower contact. In addition to the ocelli, felsic layers and felsic lenses exist within the sill (Philpotts, 1972).

Within the sill, there were five prominent feldspathic unit layers, which Philpotts (1972) refers to as felsic. Starting from the top contact of the sill, a felsic layer at 512 cm, with respect to the bottom of the sill, runs the entire length of the quarry and is not more than 1 cm thick. Between 485 cm and 500 cm, the ocelli within have a diameter of 5 mm and are intermixed with felsic lenses that range from 3-10 cm long. The third felsic layer is at 485 cm and is approximately 5 mm thick with a flat base and diapiric structures that are tilted slightly and on average, rise 2 cm above the layer. Philpotts notes that anywhere a diapiric structure reaches above 2 cm from the layer, the diapir structure cuts off and becomes a separate globular mass up to several centimeters in diameter. At 430 cm, there is a prominent felsic layer of a continuous sheet roughly 1 cm thick with a flat bottom and a domed upper surface. The last felsic layer that exists within the sill occurs at 385 cm above the lower contact. On average, this layer is up to 10 cm thick and runs the entire length of the sill. It has a relatively flat lower surface and a bulbous upper surface with domes that are larger than other parts of the sill (Philpotts, 1972).

1.7 Hypotheses for the Origin of Ocelli and Felsic Units

Philpotts (1972) proposed three different hypotheses for the origin of the ocelli:

1. Fragments of feldspathic country rock were incorporated into the fourchite magma and melted, however due to slow diffusion rates, the fragments were not entirely assimilated.

2. Gas cavities present in the magma may have provided a space where residual felsic components migrated to, causing an appearance that could be interpreted as an immiscible liquid.
3. An immiscible felsic liquid separated out from the fourchite magma.

Philpotts argues that the most unlikely hypothesis is that of the incorporation of the fragments of feldspathic rock. Within the sill, there is a zone that contains many xenoliths of feldspathic sandstone which would likely provide an ideal composition for some melting fraction to occur. In addition, the high concentration of quartz within the sandstone would have most likely reacted with the highly undersaturated fourchite magma. Philpotts indicates that the lack of melting within the xenoliths and lack of ocelli material surrounding them, is a large indication that this hypothesis is least likely to have created the ocelli. The ocelli found at the bottom of the chilled margin increase in size as a function of the distance from the chilled margin. This suggests that they may have separated as a different liquid and grown from the host fourchite magma. The ocelli gradually decrease and at 15 centimeters above the margin, they completely disappear. He suggests that the gradual change in size and numbers would be difficult to explain if the ocelli had been a product of the random xenolith inclusions within the magma. Additional isotopic and rare earth analyses indicate that the fourchite and ocelli are genetically related. Both the fourchite and ocelli have a Sr^{87}/Sr^{86} ratio of 0.704 which suggests that there was little to no contamination from crustal material, discrediting the first hypothesis (Philpotts, 1972).

The ocelli's size and distribution in addition to the minor element data do not completely rule out the second hypothesis. Philpotts suggests that if the gas cavity hypothesis were to have led to the origin of the ocelli, high gas pressures would have been required to support the open spaces. Once the host fourchite solidified and the gas pressures decreased, only then would the

residual liquids have been able to migrate to fill these cavities. However, the thick felsic sheet that exists 385 cm contains diapiric structures that rise from the surface of the layer into the overlying fouchite rock. Since the fouchite deformed in such a way that allowed the diapiric structures to form, Philpotts argues that this occurrence negates the condition that the surrounding rock had enough strength before the remaining liquid was able to fill the gas cavities. Regardless if the ocelli originated from filling gas cavities or from droplets of an immiscible liquid, there had to have been an initial separation of an immiscible phase.

This initial separation of the immiscible phase would cause ocelli to grow and exist within the fouchite. Philpotts uses the distribution and shapes of the ocelli and felsic units to make approximate calculations of the viscosity and density of the immiscible phase and fouchite magma. Using Stokes Law, found in Appendix A, Philpotts was able to quantify the velocity in which the initial ocelli phase rose through the host fouchite magma. He found that the density of the immiscible silicate liquid was 2.10 g/cm^3 while the host fouchite was 2.54 g/cm^3 (Philpotts, 1972). This data suggesting that the ocelli had risen up through the more dense fouchite magma, which validates the diapiric structures seen at 385 cm above the bottom sill margin. The less-dense, immiscible silicate liquid was able to float towards the top of the sill and accumulate into large lens-shaped masses. Based upon the results of viscosity and density, Philpotts states that these properties correspond to a silicate magma, ruling out the first two hypotheses and suggesting that the ocelli within the Ste. Dorothée Sill formed from an immiscible silicate liquid (Philpotts, 1972).

2 METHODS

2.1 Overview

Philpotts (1972) provided descriptions of the Ste. Dorothée sill in the excavated quarry before it was filled again. I use the bulk rock analyses of Philpotts (1972) and the alphaMELTS program (Antoshechkina et al., 2012) to test the hypothesis of liquid immiscibility as the origin for the ocelli in the Ste. Dorothée sill. A description of the alphaMELTS program and how the program works is provided in the Modeling section of this thesis.

In order to test his hypothesis, the composition of the magma before liquid separation has to be estimated. I used the descriptions and stratigraphy of the sill provided by Philpotts (1972) to estimate the relative proportions of ocelli and of felsic layers in the sill. The ocelli and felsic layers were both considered to be the same separated liquid. Calculation of the proportion of ocelli in the sill was separated into eight different sets based upon the various layers where ocelli are present in the sill. Calculation of the proportion of felsic layers in the sill was separated into five different sets corresponding to the five prominent felsic layers in the sill. The calculations start from the top of the sill and work downward towards the bottom contact. I estimated the volume proportions of ocelli and felsic lenses for the entire 5.45 m of exposed sill. Refer to Figure 1.10 in the introduction, which shows the sill stratigraphy.

2.2 Volume Calculations for Ocelli

Ocelli in 545-530 cm: The ocelli were described as no larger than 2 mm in diameter at maximum size and decreasing in size towards the chilled margin. I assume that the average diameter was 1 mm. I also assumed the ocelli were all spherical, and used the sphere volume equation, $V = \frac{4}{3}\pi r^3$ to estimate their volume. Since no frequency of the ocelli was mentioned in any paper for the first 15 cm of the sill, I assumed a frequency of one ocelli per cubic centimeter.

Ocelli in 530-512 cm: The ocelli between 15 cm and 33 cm decrease in frequency. To account for this, the radius used for the volume calculation was reduced in an equal steps from 0.5 mm to 0 for the 18 cm thick layer. The volume equation was used for each of the 18 steps and the results were added together.

Ocelli in 512-500 cm: Ocelli have diameters of 3 mm in this layer and I assume a frequency of one ocelli per cubic centimeter.

Ocelli in 500-485 cm: Ocelli have diameters of 5 mm and I assume a frequency of one ocelli per cubic centimeter.

Ocelli in 485-445 cm: Ocelli of 5 mm in diameter exist in this layer. Philpotts (1972) states that two concentrated layers of ocelli exist in this section, however no frequency is given. I disregard the concentrated layers and assume a frequency of one ocelli per cubic centimeter. Similar to the way the ocelli volumes were calculated between 15cm and 33 cm, the radius gradually decreases from 2.5 mm to 0 in 40 equal steps to account for a decrease in abundance.

Ocelli in 445-385 cm: The ocelli in this layer was described as 1cm in diameter on average. Keeping with aforementioned assumptions, the total volume of ocelli for this layer was calculated to be 3141.59 cm^3 .

Ocelli in 385-370 cm: Ocelli in this layer are described to have a radius of 2.5 mm, gradually decreasing in abundance. Since no value is given for frequency of the ocelli, I decrease the radius for calculations in an equal step interval starting from a radius of 2.5 mm to 0 mm.

Ocelli in 15-0 cm: The calculations for this layer used Philpotts' (1972) graph, represented by Figure 1.10, based upon the logarithmic concentration of ocelli/ cm^3 versus the logarithm of the distance up from the lower contact of the sill. First, the values were calculated

Table 2.1: Calculations of Ocelli by Layer		
Layer (cm) From Top Contact	Assumption	Volume (cm^3)
545-530	Frequency of ocelli at one per cubic centimeter	78.5
530-512	Decrease in ocelli size based on equal intervals and a frequency of one per cubic centimeter	26.2
512-500	Frequency of ocelli at one per cubic centimeter	1696.4
500-485	Frequency of ocelli at one per cubic centimeter	9817.5
485-445	Decrease in ocelli size based on equal intervals and a frequency of one per cubic centimeter	6876.3
445-385	Frequency of ocelli at one per cubic centimeter	314159.2
385-370	Decrease in ocelli size based on equal intervals and a frequency of one per cubic centimeter	4424.4
15-0	Using Figure 1.10 as a basis for the concentration and size of ocelli	309.4
		Total:
		337388.1

from log values back to ocelli/ cm^3 and distance in centimeters. From then, each centimeter volume could be calculated.

Table 2.1 shows the volume totals for each layer described above based upon my assumptions.

2.3 Calculations for Felsic Units

Five separate calculations were made to estimate the total volume of felsic material that exists within the Ste. Dorothee Sill. Not having access to the sill, I resorted to photo analysis and Philpotts' (1972) descriptions to calculate felsic unit volumes. I defined the area calculated for each of the layers as being $10,000\text{ cm}^2$, or $100 \times 100\text{ cm}$, and multiplied by the thickness of the specified felsic layer or units. The calculations were made as follows:

Felsic Layer 1 at 512 cm: The felsic layer has a thickness of 1 cm and extends throughout the entirety of the sill for a total volume of $10,000\text{ cm}^3$.

Felsic Layer 2 between 485 cm and 500 cm: This layer within the sill contained felsic units that ranged between 3-10 cm long (Figure 2.1). I estimated the proportion of felsic units in

Figure 2.1 to be 15%. This percentage then extrapolated over the 15 cm layer came out to 22,500 cm^3 .

Felsic Layer 3 at 500 cm: Using the image seen in Figure 2.2 as reference from Philpotts' (1972) paper, I was able approximate the volume. The block in the image shown is 10x12x7 cm. Descriptions of the domes give relative spacing of 5 domes per block. I simplified the calculations and used the volume of a sphere equation with a radius of 0.5 cm each. At the bottom of this section was a 0.25 cm thick felsic layer as well. These two values were added together and came out to 32.6 cm^3 . I then had to take the 10x12x7 volume and calculate what the volume would be over the 100x100 cm area. The total volume for this area came out to 2718.17 cm^3 .



Figure 2.1: Image showing Felsic Layer 2 between 485 cm and 500 cm from the bottom of the sill. This image is used to approximate the volume based on the felsic units, seen as the white material in this photo (Philpotts, 1972).

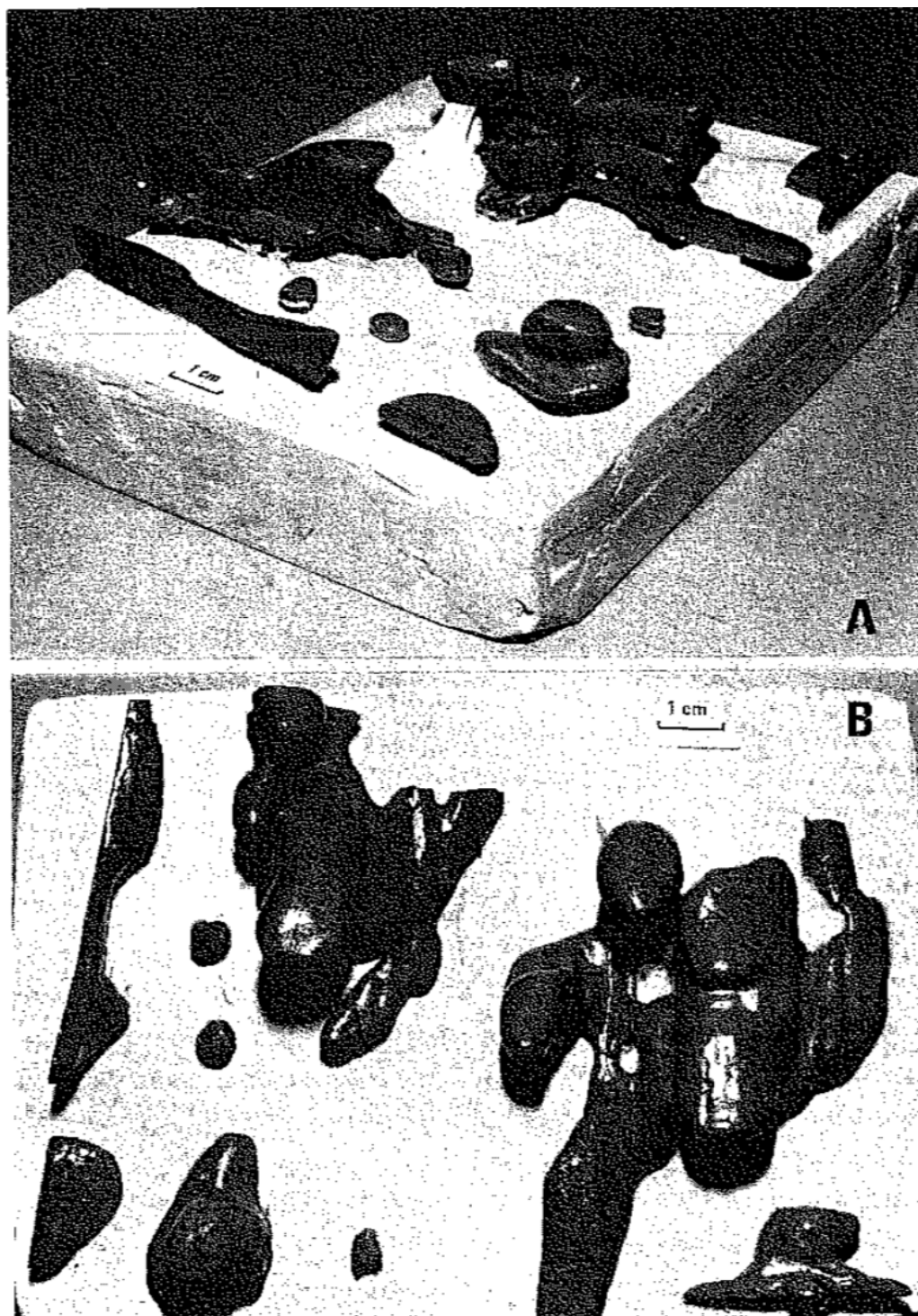


Figure 2.2: Image showing a representation of Felsic Layer 3 at 500 cm above the bottom chilled margin. This diagram was created by cutting a block from this section of the sill into thin slices so the diapiric felsic structures could be traced (Philpotts, 1972).

Felsic Layer 4 at 430 cm: In this section, there is a consistent 1 cm thick felsic layer with a domed upper surface. I assume the domes occurred at the same frequency as the domes in the Felsic Layer 3, roughly 5 domes for every 10x12 cm area. Based upon this assumption, it was calculated that there are roughly 218 domes within the 100x100 cm area. Using the sphere volume equation with domes at 0.5 cm in radius and the 1 cm thick felsic layer, I add the two values together to get a total volume of 10218.17 cm^3 .

Felsic Layer 5 at 385 cm: Philpotts (1972) states that this layer is up to 10 cm thick in areas with variation. I assume an average thickness of 6 cm, the layer was simply calculated over the 100x100 cm area multiplied by 6 to get a total volume of 60000 cm^3 for this layer.

In total, the felsic units made up 105436 cm^3 within the defined 100x100x545 cm section of the sill, or 1.9% of the sill's volume.

3 MODELING

3.1 Background of the alphaMelts Program

AlphaMELTS calculates equilibrium assemblages along a thermodynamic path defined by the user. These paths can be an adiabat, an isotherm, or a geotherm. It is suitable for multi-component systems such as anhydrous, hydrous, or water undersaturated systems. This program has the ability to perform calculations for either sub-solidus or with liquids present in the defined system. It also allows for the melting or crystallization of a defined rock composition in batches, fractionally, or continuous (Antoshechina and Asimow, 2018).

The thermodynamic model is calibrated on a wide variety of bulk compositions and other research papers outlining natural thermodynamic processes (Antoshechina and Asimow, 2018). Pressure, temperature, oxygen fugacity, calculation intervals are defined using an *environment file*. Various functions are also offered within the *environment file*, however the functions that are important to this thesis are the *Multiple Liquids* and *Fractionate Second Liquid* functions. Both of these functions are used in an attempt to look at the possibility of liquid immiscibility within a bulk rock composition, specifically Philpotts (1972). The *Fractionate Second Liquid* function will treat all liquids as fractioning phases, and remove them from the calculations as they crystallize. The *Multiple Liquids* function is able to see exsolution of immiscible liquids, and is able to indicate and separate out liquids that coexist within a melt.

A *bulk composition file* is used to define the composition of a starting magma. The *bulk composition file* and the *environment file* are used in tandem to set all of the conditions needed to run the calculations. The output that is created from the calculations includes modes and compositions for all solid and liquid phases including other thermodynamic data such as density and viscosity measurements (Antoshechina and Asimow, 2018). The program is run through the

terminal window (Mac OSX) and all outputs are text files which can be converted to Excel files for interpretation.

3.2 Isobaric Experimental Trials

Bulk composition data was taken from Philpotts (1972) and represented in a *Melts file*. Using Philpotts' (1972) bulk composition data for the ocelli and host fourchite, various relative weight percentages of ocelli and fourchite were tested as parental melt composition. The trials were run at 2, 5, 10, 20, and 50 wt. % ocelli composition relative to host fourchite, seen in Table 3.1. These trials were run three different ways, varying only with two of the settings in the *environment file*. The first test used the *Multiple Liquids* setting on, the second with both the *Multiple Liquids* and *Fractionate Second Liquid* functions turned on, and the third with both turned off. In total, twelve runs were completed for the experiments.

3.2.1 Parental Liquid Composition

To calculate the relative proportions of oxides for the parent magmas the bulk composition of the ocelli/felsic units were multiplied by the respective percent abundance in the whole magma. For example, each of the components within the bulk composition data for the ocelli/felsic units was scaled to 2% abundance whereas the fourchite composition was scaled to 98%. These values were then added together to form an estimate as to the composition of the parent magma. Estimated values for the parent magma in each trial can be seen in Table 3.1. I focus strictly on the MC2 and MC10 data sets, corresponding to the values in Table 3.1. The MC2 proportions are representative of Goldie's (1972) calculated values and the MC10 is the closest proportion of ocelli to host fourchite in my volume calculations.

Based on his field observations, Philpotts considered that liquid immiscibility must have occurred after the emplacement of the sill. This isobaric trials are designed to test thi hypothesis.

Table 3.1
Norms of the fourchite (F) and the ocelli (O) found in the Stc. Dorothée sill. The actual norms given by Philipotts (1972) are seen in the 'Actual' column. The weight percentages from each of the tests were calculated by the ocelli volume from the sill and then normalized to run the total composition for the alphaMELTS program.

Ocelli wt. %	Actual			2%			5%			10%			20%			30%			50%			
	F	O	Total	F	O	Total	F	O	Total	F	O	Total	F	O	Total	F	O	Total	F	O	Total	
Norm																						
SiO₂	42.94	51.57	43.1126	42.0812	1.0314	43.1126	40.793	2.5785	43.3715	38.646	5.157	43.803	34.352	10.314	44.666	30.058	15.471	45.529	21.47	25.785	47.255	
TiO₂	3.48	1.91	3.4486	3.4104	0.0382	3.4486	3.306	0.0955	3.4015	3.132	0.191	3.323	2.784	0.382	3.166	2.436	0.573	3.009	1.74	0.955	2.695	
Al₂O₃	16.26	20.84	16.3516	15.9348	0.4168	16.3516	15.447	1.042	16.489	14.634	2.084	16.718	13.008	4.168	17.176	11.382	6.252	17.634	8.13	10.42	18.55	
Fe₂O₃	5.5	1.2	5.414	5.39	0.024	5.414	5.225	0.06	5.285	4.95	0.12	5.07	4.4	0.24	4.64	3.85	0.36	4.21	2.75	0.6	3.35	
FeO	5.25	2.76	5.2002	5.145	0.0552	5.2002	4.9875	0.138	5.1255	4.725	0.276	5.001	4.2	0.552	4.752	3.675	0.828	4.503	2.625	1.38	4.005	
MnO	0.3	0.16	0.2972	0.294	0.0032	0.2972	0.285	0.008	0.293	0.27	0.016	0.286	0.24	0.032	0.272	0.21	0.048	0.258	0.15	0.08	0.23	
MgO	3.96	1.1	3.9028	3.8808	0.022	3.9028	3.762	0.055	3.817	3.564	0.11	3.674	3.168	0.22	3.388	2.772	0.33	3.102	1.98	0.55	2.53	
CaO	10.35	4.86	10.2402	10.143	0.0972	10.2402	9.8325	0.243	10.0755	9.315	0.486	9.801	8.28	0.972	9.252	7.245	1.458	8.703	5.175	2.43	7.605	
Na₂O	5	7.25	5.045	4.9	0.145	5.045	4.75	0.3625	5.1125	4.5	0.725	5.225	4	1.45	5.45	3.5	2.175	5.675	2.5	3.625	6.125	
K₂O	2.28	3.54	2.3052	2.2344	0.0708	2.3052	2.166	0.177	2.343	2.052	0.354	2.406	1.824	0.708	2.532	1.596	1.062	2.658	1.14	1.77	2.91	
H₂O +	3.33	4.36	3.3506	3.2634	0.0872	3.3506	3.1635	0.218	3.3815	2.997	0.436	3.433	2.664	0.872	3.536	2.331	1.308	3.639	1.665	2.18	3.845	
P₂O₅	0.95	0.12	0.9334	0.931	0.0024	0.9334	0.9025	0.006	0.9085	0.855	0.012	0.867	0.76	0.024	0.784	0.665	0.036	0.701	0.475	0.06	0.535	
CO₂	0.77	0.67	0.768	0.7546	0.0134	0.768	0.7315	0.0335	0.765	0.693	0.067	0.76	0.616	0.134	0.75	0.539	0.201	0.74	0.385	0.335	0.72	
S	0.09	0.11	0.0904	0.0882	0.0022	0.0904	0.0855	0.0055	0.091	0.081	0.011	0.092	0.072	0.022	0.094	0.063	0.033	0.096	0.045	0.055	0.1	
Total:	100.46	100.45	100.459	98.4508	2.009	100.459	95.437	5.0225	100.4595	90.414	10.045	100.459	80.368	20.09	100.458	70.322	30.135	100.457	50.23	50.225	100.455	

He estimated the pressure of emplacement to be 300 bars, and he estimated the temperature of emplacement of the sill to be 1100°C and the sill have been largely solid by 1000°C (Philpotts, 1972). I performed all trials at 300 bars and used a starting temperature of 1900°C to ensure a complete liquid magma with a final temperature of 400°C to sure complete solidification. I used cooling steps of 5°C.

3.3 Isentropic Experimental Trials

If we allow for liquid separation to occur during melt transport before the sill is emplaced, an isentropic model can be used in the alphaMELTS program. The *isentropic mode* allows for a change in pressure and temperature, but preserves entropy of the system. Since Philpotts (1972) does not comment on the source of the magma, I assumed that the parental magma originated near the base of the crust, corresponding to a pressure of 1 GPa and 1000°C, reasonable estimates for the conditions at the base of the crust. In a perfect system, isentropic processes conserve the total entropy, not allowing heat to enter or leave the system (Kieffer and Delany, 1979). In these trials, perfect entropy is not observed and some heat does leave the system. Then, by decreasing the pressure to 0.03 GPa (300 bars), it would simulate the transport of the magma from a deeper source to the suggested emplacement depth. The isentropic model can be represented in Figure 3.1 (HMXXEarthScience).

Once the parent magmas in each trial reaches the suggested emplacement pressure of 300 bars, I cooled the remaining liquids to track the minerals that would precipitate from the melt in addition to any immiscible liquids that may separate from the melt. To ensure consistency in the model, I cooled each of the respective remaining liquids from the parent magmas from MC2 and MC10 at the temperature in which they reached the emplacement pressure of 300 bars. I allowed

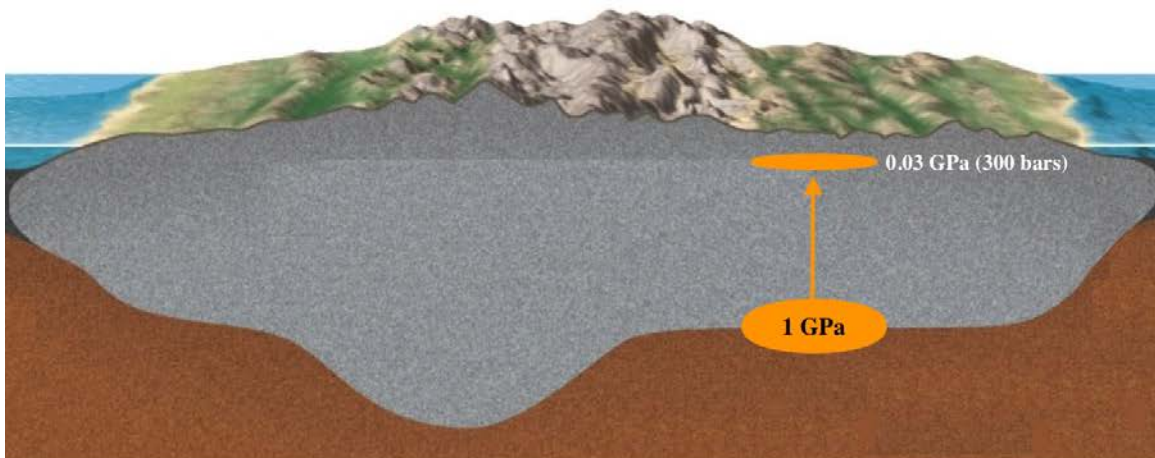


Figure 3.1: This diagram shows a visualization of the isentropic model. The pressures used to constrain the program directly correlate to depth in the crust. 1 GPa implies the depth at the base of the crust and 300 bars represents Philpotts' (1972) suggested depth of emplacement. (HMX Earth Science).

the program to calculate any immiscible liquids that would separate immiscible liquids by turning on the *Multiple Liquids* and *Fractionate Second Liquid* functions.

After the trials, I then take the mineralogy and compositional data from the separated liquids and compare those to the data that Philpotts (1972) provides in his paper. The mineral groups that alphaMELTS calculates during crystallization have chemical formulas that I then use to compare to the specific minerals described for the Ste. Dorothee sill and other intrusions in the Monteregean Hills igneous province. Each of the separate liquids calculated for the isentropic trials are compared to Philpotts (1972) composition for the ocelli.

4 RESULTS

4.1 Crystallization in the Upper Crust

The isobaric model attempts to represent the conditions of the sill after it had been emplaced. Any separation of an immiscible liquid is considered to occur post-emplacment of the sill. The only variable changing in these trials is the temperature, allowing these results to focus on the mineralogical composition of the sill. The results from the isobaric trials did not yield multiple liquids that resembled the bulk rock composition provided by Philpotts (1972). However, immiscible liquids separated out of the initial melt in both MC2 and MC10. I present the results of the trials in data sets that show the separated liquids and mineralogy of both MC2 and MC10. The compositions of the immiscible liquids are based on the calculations of the alphaMELTS software and the mineralogical compositions are based upon thermodynamic data calculated through the program.

Shown in Figure 4.1 A, clinopyroxene is the first group of minerals that crystallize from the starting liquid, followed by other mineral groups. Table 4.1 shows the temperature at all of the various mineral groups crystallize out of the melt. There are slight variations between MC2 and MC10 in regards to crystallized minerals by their respective final temperatures. Minerals such as olivine and nepheline begin to crystallize in the total melt but are reabsorbed. Both the MC2 and MC10 trials are run until the program fails due to unknown reasons. This leaves 3.6 wt. % of initial liquid left over for MC2 and 9.0% at the end of MC10.

4.1.1 Modal Mineralogy

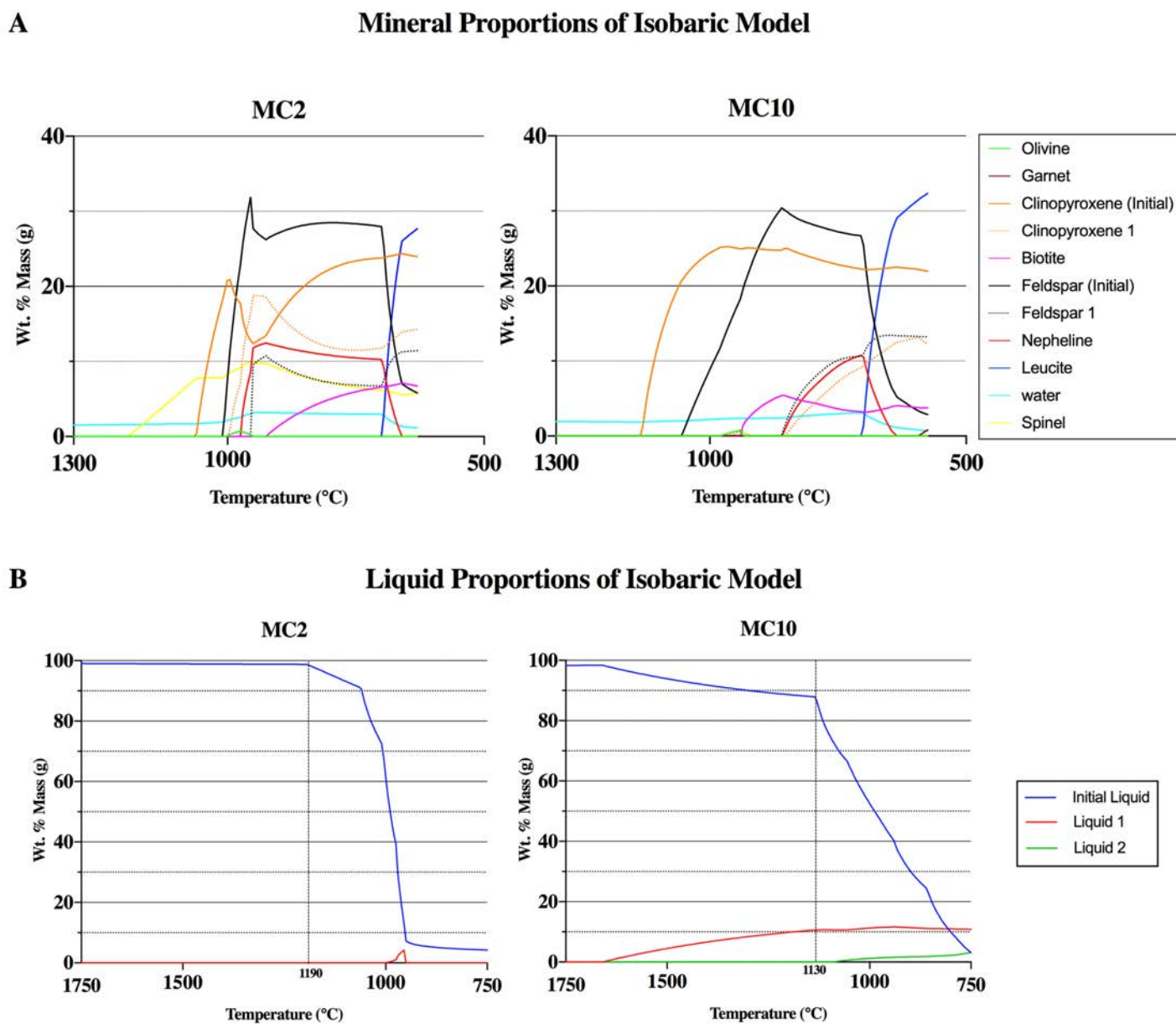


Figure 4.1: (A) Graphs showing the wt. % vs. Temperature of the proportions of minerals to crystallize out from the initial liquid in each of the isobaric trials. The trials end at different temperatures due to calculation failure in the alphaMELTS software. (B) Proportions of liquids separated from the isobaric trials are shown in a Wt. % vs Temperature graph. The dashed line in each of the graphs represent the temperature at which minerals first begin to crystallize from the initial melt. Only one liquid separated from MC2, whereas two separate from MC10. Liquid 1 from MC10 separates before any crystallization occurs.

Table 4.1 Isobaric Crystallization of Trials MC2 and MC10					
Trial	Wt. %	°C	Mineral Group	Formula	Mineral
MC2	5.80	1190	Spinel	$(Fe^{2+}_{0.96}Mg_{0.05}Fe^{3+}_{1.92}Al_{0.06}Ti_{0.01})O_4$	Magnetite
MC2	0*	1000	Olivine	$(Ca_{0.01}Mg_{0.72}Fe^{2+}_{0.20}Mn_{0.08}Co_{0.00}Ni_{0.00})_2SiO_4$	Forsterite
MC2	5.80	1005	Feldspar (Initial)	$K_{0.03}Na_{0.63}Ca_{0.34}AlSi_{2.66}O_8$	Plagioclase
MC2	11.4	950	Feldspar 1	$K_{0.79}Na_{0.20}Ca_{0.01}AlSi_3O_8$	Orthoclase
MC2	23.9	1060	Clinopyroxene (Initial)	$Na_{0.04}Ca_{0.96}Fe^{2+}_{0.22}Mg_{0.30}Fe^{3+}_{0.10}Ti_{0.40}Al_{0.83}Si_{1.15}O_6$	Titanaugite
MC2	14.3	995	Clinopyroxene 1	$Na_{0.10}Ca_{0.90}Fe^{2+}_{0.20}Mg_{0.53}Fe^{3+}_{0.14}Ti_{0.03}Al_{0.33}Si_{1.79}O_6$	Augite
MC2	6.70	920	Biotite	$K(Fe^{2+}_{0.29}Mg_{0.71})_3AlSi_3O_{10}(OH)_2$	Biotite
MC2	0*	970	Nepheline	$Na_{2.76}K_{0.56}Ca_{0.34}Al_4Si_4O_{16}$	Nepheline
MC2	27.6	695	Leucite	$K_{0.00}NaAlSi_2O_{5.20}(OH)_{1.61}$	Analcime
MC10	3.70	935	Biotite	$K(Fe^{2+}_{0.21}Mg_{0.79})_3AlSi_3O_{10}(OH)_2$	Biotite
MC10	0*	975	Olivine	$(Ca_{0.00}Mg_{0.86}Fe^{2+}_{0.10}Mn_{0.04}Co_{0.00}Ni_{0.00})_2SiO_4$	Forsterite
MC10	0.80	590	Garnet	$(Ca_{0.94}Fe^{2+}_{0.03}Mg_{0.03})_3Al_2Si_3O_{12}$	Garnet
MC10	2.80	1055	Feldspar (Initial)	$K_{0.01}Na_{0.41}Ca_{0.57}Al_{1.57}Si_{2.43}O_8$	Plagioclase
MC10	13.2	855	Feldspar 1	$K_{0.88}Na_{0.12}Ca_{0.01}Al_{1.01}Si_3O_8$	Orthoclase
MC10	22.9	1130	Clinopyroxene (Initial)	$Na_{0.12}Ca_{0.98}Fe^{2+}_{0.15}Mg_{0.36}Fe^{3+}_{0.07}Ti_{0.43}Al_{0.90}Si_{1.10}O_6$	Titanaugite
MC10	12.3	965	Clinopyroxene 1	$Na_{0.06}Ca_{0.94}Fe^{2+}_{0.11}Mg_{0.67}Fe^{3+}_{0.07}Ti_{0.01}Al_{0.32}Si_{1.82}O_6$	Augite
MC10	0*	855	Nepheline	$Na_{2.69}K_{0.56}Ca_{0.38}Al_4Si_4O_{16}$	Nepheline
MC10	32.3	700	Leucite	$K_{0.00}NaAlSi_2O_{5.12}(OH)_{1.77}$	Analcime

* Denotes minerals that begin to precipitate from the initial liquid but are reabsorbed before alphaMELTS completes the calculations

All mineral groups produced by alphaMELTS were validated by comparing to CITATION

While similar mineral groups crystallize for each of the initial liquids, the wt. % of the mineral groups are slightly different in each data set. The point where the total melt begins to crystallize occurs at 1190°C for MC2 and 1135°C for MC10. The first mineral group to precipitate from MC2 is spinel, followed by the other mineral groups at the temperatures shown in Table 4.1. During crystallization, both the feldspar and clinopyroxene groups undergo phase separation labeled Feldspar 1 and Clinopyroxene 1, respectively. During the MC10 trial, clinopyroxene is the first mineral group to precipitate from the initial liquid. Similar to the MC2 data set, both Feldspar and Clinopyroxene undergo phase separation in MC10, producing a separate composition of each.

During the MC2 trial, only one liquid is seen to separate from the initial melt. The separation occurs at 1000°C, however it is reincorporated back into the melt at 955°C. Liquid 1 separates from MC10 at 1655°C and Liquid 2 separates at 1085°C. Figure 1.4 B shows the separated liquids and their proportions compared to the initial liquids. During the trials, alphaMELTS stops calculating at different temperatures due to calculation failures. For MC2, the calculations stop at 630°C while MC10 stops at 575°C.

4.1.2 Immiscible Liquids from Isobaric Trials

In both the MC2 and MC10 data sets, immiscible liquids are only found to separate when *Multiple Liquids* or *Fractionate Second Liquid* functions are turned on. The compositions of all separated liquids from both MC2 and MC10 are represented in Figure 4.2. All three of the liquids separated from the MC2 and MC10 have unique proportions of oxides. Liquid 1 from the MC2 data set initially separates out with a high proportion of silica, CO_2 , and CaO , however as temperature continues to decrease, the content of CaO and P_2O_5 increase becoming the dominant oxides along with SiO_2 . Liquid 1 from MC10 begins with high proportion of iron oxides. At 700°C, the compositions of both immiscible liquids and the initial liquid. Liquid 2 from MC10 has high proportions of calcium and phosphorous oxides with very low proportions of every other oxide. Due to numerous failures of the alphaMELTS program, modal mineralogy could not be determined for the separated liquids from either the MC2 or MC10 data sets.

Immiscible Liquids from Isobaric Experiments

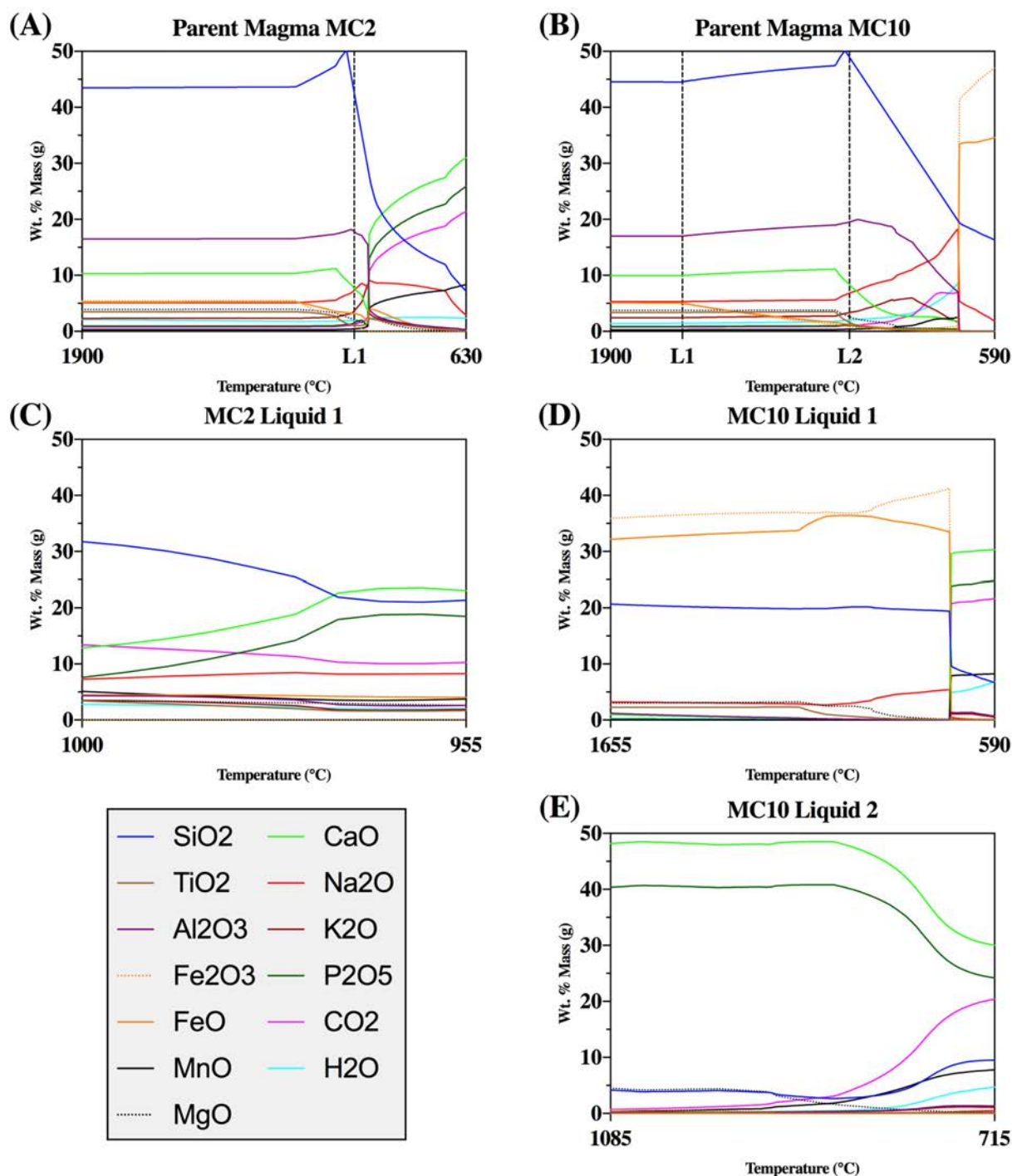


Figure 4.2: Each of the diagrams show the proportions of oxides in the immiscible liquids calculated during the isobaric experiments. Each of the immiscible liquids separate from the parental magma at different temperatures so the x-axis on each graph varies. Some liquids separate from the melt, but are reabsorbed back into the parental magma at a lower temperature (A) Parent magma of MC2 (B) Parent magma of MC10 (C) Liquid 1 from MC2. This liquid initially separates from the parent magma but is reabsorbed at 955°C. (D) Liquid 1 from MC10. (E) Liquid 2 from MC10 which is reabsorbed back into the initial melt at 715°C.

4.2 Melt Ascent from Source Region

Since the isobaric trials did not yield liquids that resembled those from Philpotts (1972) paper, I used an isentropic model to look at where the total melt would have originated. Assuming the melt originated at the base of the crust, an adiabatic ascent (isentropic) model that begins at 1GPa and slowly depressurizes to the suggested emplacement of 0.03 GPa is used in addition to the accepted temperature of 1000°C for the starting depth. In both the MC2 and MC10 data sets, there is no liquid separation from either initial melt. Even in trials where the *Multiple Liquids* and *Fractionate Second Liquid* functions are turned on, no liquids separate out.

Table 4.2: MC2 Ascent From 1GPa		
Mineral	Wt. %	Formula
Biotite	2.02	$K(Fe^{2+}_{0.20}Mg_{0.80})_3AlSi_3O_{10}(OH)_2$
Feldspar	12.84	$K_{0.05}Na_{0.55}Ca_{0.41}Al_{1.41}Si_{2.59}O_8$
Clinopyroxene (Initial)	22.04	$Na_{0.04}Ca_{0.94}Fe^{2+}_{0.13}Mg_{0.50}Fe^{3+}_{0.12}Ti_{0.30}Al_{0.63}Si_{1.35}O_6$
Clinopyroxene 1	1.51	$Na_{0.05}Ca_{0.92}Fe^{2+}_{0.13}Mg_{0.64}Fe^{3+}_{0.11}Ti_{0.11}Al_{0.37}Si_{1.67}O_6$
Spinel	8.32	$Fe^{2+}_{0.92}Mg_{0.30}Fe^{3+}_{1.32}Al_{0.24}Cr_{0.00}Ti_{0.22}O_4$
Apatite	0.00*	$Ca_5(PO_4)_3OH$

* Denotes minerals that begin to precipitate during ascent, but are reabsorbed into the melt

Table 4.3: MC10 Ascent From 1GPa		
Mineral	Wt. %	Formula
Biotite	0.00*	$K(Fe^{2+}_{0.19}Mg_{0.81})_3AlSi_3O_{10}(OH)_2$
Feldspar	19.9	$K_{0.06}Na_{0.55}Ca_{0.39}Al_{1.39}Si_{2.61}O_8$
Clinopyroxene (Initial)	18.4	$Na_{0.04}Ca_{0.94}Fe^{2+}_{0.12}Mg_{0.51}Fe^{3+}_{0.11}Ti_{0.30}Al_{0.63}Si_{1.35}O_6$
Clinopyroxene 1	4.00	$Na_{0.05}Ca_{0.92}Fe^{2+}_{0.13}Mg_{0.65}Fe^{3+}_{0.10}Ti_{0.11}Al_{0.36}Si_{1.68}O_6$
Spinel	8.38	$Fe^{2+}_{0.93}Mg_{0.30}Fe^{3+}_{1.25}Al_{0.24}Cr_{0.00}Ti_{0.25}O_4$
Apatite	0.00*	$Ca_5(PO_4)_3OH$

* Denotes minerals that begin to precipitate during ascent, but are reabsorbed into the melt

However, some mineral groups do precipitate out from the melt during the ascent from 100 kb to 0.3 kb. The remaining liquid from the MC2 and MC10 trials was then cooled through the isobaric model to crystallize the rest of the liquid. The remaining liquid, when cooled under constant pressure, produced two separate liquids. The separate liquids from the isobaric model after the adiabatic ascent are different in composition to the liquids that separated out in the strictly isobaric trials.

In the MC2 isentropic model, mineral groups that precipitate from the melt are similar to those from MC10. Biotite, feldspar, two phases of clinopyroxene, spinel, and apatite all precipitate from the melt. However, apatite crystallizes during the ascent, but is reabsorbed back into the melt. Table 4.2 shows the mineral groups that precipitate out of MC2 during ascent and the wt. % of each mineral. At the end of the ascent from 1 GPa to 300 bars, 39 wt. % of the initial melt remained liquid.

In the MC10 isentropic model, mineral groups such as clinopyroxene, biotite, feldspar, apatite, and spinel precipitate out of the ascending melt. The chemical formulas for minerals that precipitate out are shown in Table 4.3. The initial clinopyroxene underwent a phase separation that produced clinopyroxene 1. The proportions of magnesium, titanium, aluminum, and silicon is slightly varied between the two phases of clinopyroxene, where the other elements in the mineral stay relatively similar. At the end of the ascent from 1 GPa to 300 bars, 41 wt. % of the initial melt remained liquid.

4.2.1 Crystallization of Remaining Liquid from Isentropic Trials

After each of the remaining liquids from both the MC2 and MC10 reached the suggested emplacement pressure of 300 bars during the isentropic model, they were cooled for the remaining liquid to crystallize. The bulk composition of both remaining liquids from the MC2

and MC10 isentropic trials are seen in Table 4.4 compared to the composition of ocelli from Philpotts (1972). The minerals that precipitate out are shown in Table 4.5. Slight variations are seen in the chemical compositions of the minerals, however the most dominant mineral groups in each data set to precipitate are leucite, clinopyroxene, and feldspar. This is consistent between both the MC2 and MC10 data sets for this model. I chose the starting temperature and pressure based on the ending pressure and temperature of the isentropic trials for consistency.

At these starting conditions, feldspar and both phases of clinopyroxenes had already crystallized from the remaining melts. In MC2, both feldspar and clinopyroxene had already begun to crystallize at the beginning of the trials. In MC10, only clinopyroxene began crystallizing at the start of the trial. In both trials, leucite is the most dominant mineral proportionally to the other mineral groups. The clinopyroxene and feldspar groups are the most dominant after leucite. Figures 4.3 and 4.4 show how the mineral proportions of each trial change during crystallization. Some mineral groups begin to crystallize, go back into solution, then crystallize again.

Oxides	MC2	MC10	Philpotts (1972)
<i>SiO₂</i>	51.6	51.8	51.6
<i>TiO₂</i>	0.68	0.68	1.91
<i>Al₂O₃</i>	19.0	19.3	20.8
<i>Fe₂O₃</i>	1.00	1.02	1.20
<i>FeO</i>	2.71	2.67	2.76
<i>MnO</i>	0.54	0.50	0.16
<i>MgO</i>	0.78	0.76	1.10
<i>CaO</i>	4.10	4.02	4.86
<i>Na₂O</i>	8.17	8.12	7.25
<i>K₂O</i>	3.38	3.45	3.54
<i>P₂O₅</i>	0.84	0.82	0.12
<i>CO₂</i>	1.39	1.31	0.67
<i>H₂O</i>	5.73	5.60	4.36

Philpotts (1972) column shows the bulk composition data for the ocelli and felsic units

Cooling the remaining liquids from the MC2 and MC10 isentropic models yield similar results to that of the isobaric models. Two liquids separated from each of the MC2 and MC10 data. These liquids have slightly different compositions than the immiscible liquids from the isobaric trials. The compositions of these separated liquids from both MC2 and MC10 isentropic trials are seen in Figure 4.5. Liquid 1 for MC10 and MC2, have a high weight percentage of P_2O_5 , CaO , and relatively low proportions of all other oxides. By the time these liquids reach their lowest temperatures, the proportions change where CO_2 , SiO_2 , MnO have the highest proportions. Liquid 2 for each of the MC2 and MC10 data sets are iron-rich silicates, however only exist for a short amount of time during cooling.

Trial	Wt. %	°C	Mineral	Formula
MC2	1.76	530	Sphene	$CaTiSiO_5$
MC2	22.7	965	Feldspar	$K_{0.81}Na_{0.19}Ca_{0.00}AlSi_3O_8$
MC2	19.2	965	Clinopyroxene	$Na_{0.13}Ca_{0.87}Fe^{2+}_{0.35}Mg_{0.45}Fe^{3+}_{0.02}Ti_{0.01}Al_{0.25}Si_{1.93}O_6$
MC2	0.33	645	Garnet	$(Ca_{0.99}Fe^{2+}_{0.01}Mg_{0.00})_3Al_2Si_3O_{12}$
MC2	10.9	775	Nepheline	$Na_{3.06}K_{0.65}Ca_{0.14}Al_4Si_4O_{16}$
MC2	34.1	715	Leucite	$K_{0.00}NaAlSi_2O_{5.18}(OH)_{1.64}$
MC10	2.79	930	Biotite	$K(Fe^{2+}_{0.47}Mg_{0.53})_3AlSi_3O_{10}(OH)_2$
MC10	2.07	530	Sphene	$CaTiSiO_5$
MC10	26.0	945	Feldspar	$K_{0.81}Na_{0.19}Ca_{0.00}AlSi_3O_8$
MC10	16.8	970	Clinopyroxene	$Na_{0.14}Ca_{0.86}Fe^{2+}_{0.38}Mg_{0.43}Fe^{3+}_{0.05}Ti_{0.01}Al_{0.19}Si_{1.94}O_6$
MC10	15.0	860	Nepheline	$Na_{3.12}K_{0.67}Ca_{0.10}Al_4Si_4O_{16}$
MC10	26.2	705	Leucite	$K_{0.00}NaAlSi_2O_{5.19}(OH)_{1.63}$

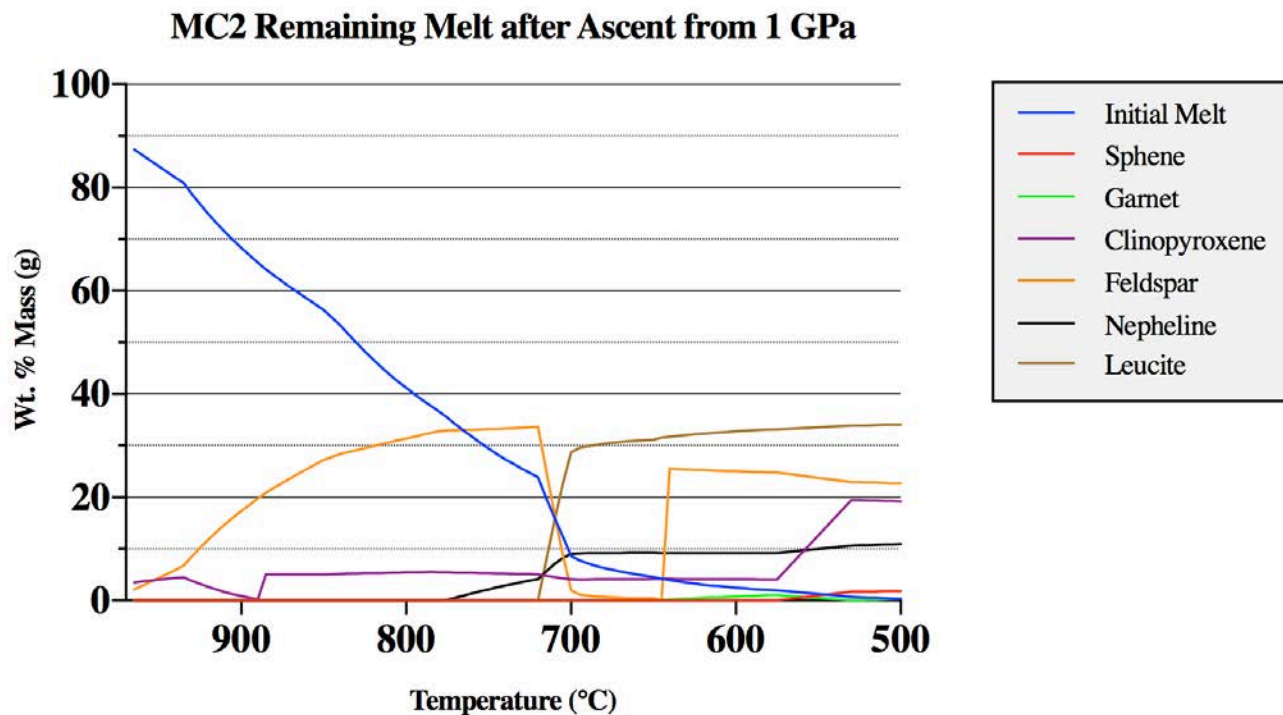


Figure 4.3: This figure shows the mineral composition for the remaining liquid in MC2 after the isentropic trial. The software uses thermodynamic and chemical data to calculate the minerals to be expected in the crystallized rock. These values are proportions of the minerals with respect to their wt. % compared to the crystallization of the liquid. Both clinopyroxene and feldspar had already begun to crystallize at the starting temperature in small proportions.

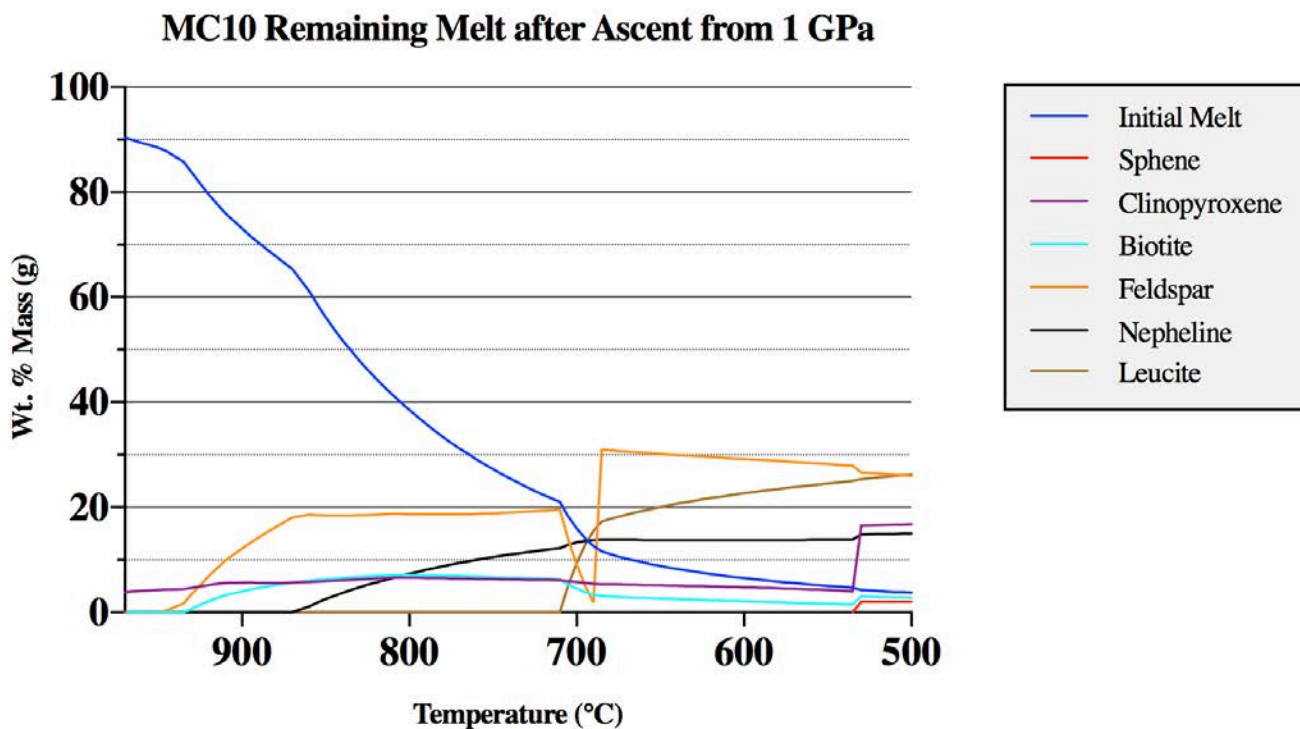


Figure 4.4: This figure shows the mineral composition for the remaining liquid in MC10 after the isentropic trial. The software uses thermodynamic and chemical data to calculate the minerals to be expected in the crystallized rock. These values are proportions of the minerals with respect to their wt. % compared to the crystallization of the liquid. Only clinopyroxene had already begun to crystallize out of the melt by the starting temperature.

Immiscible Liquids from Isentropic Model

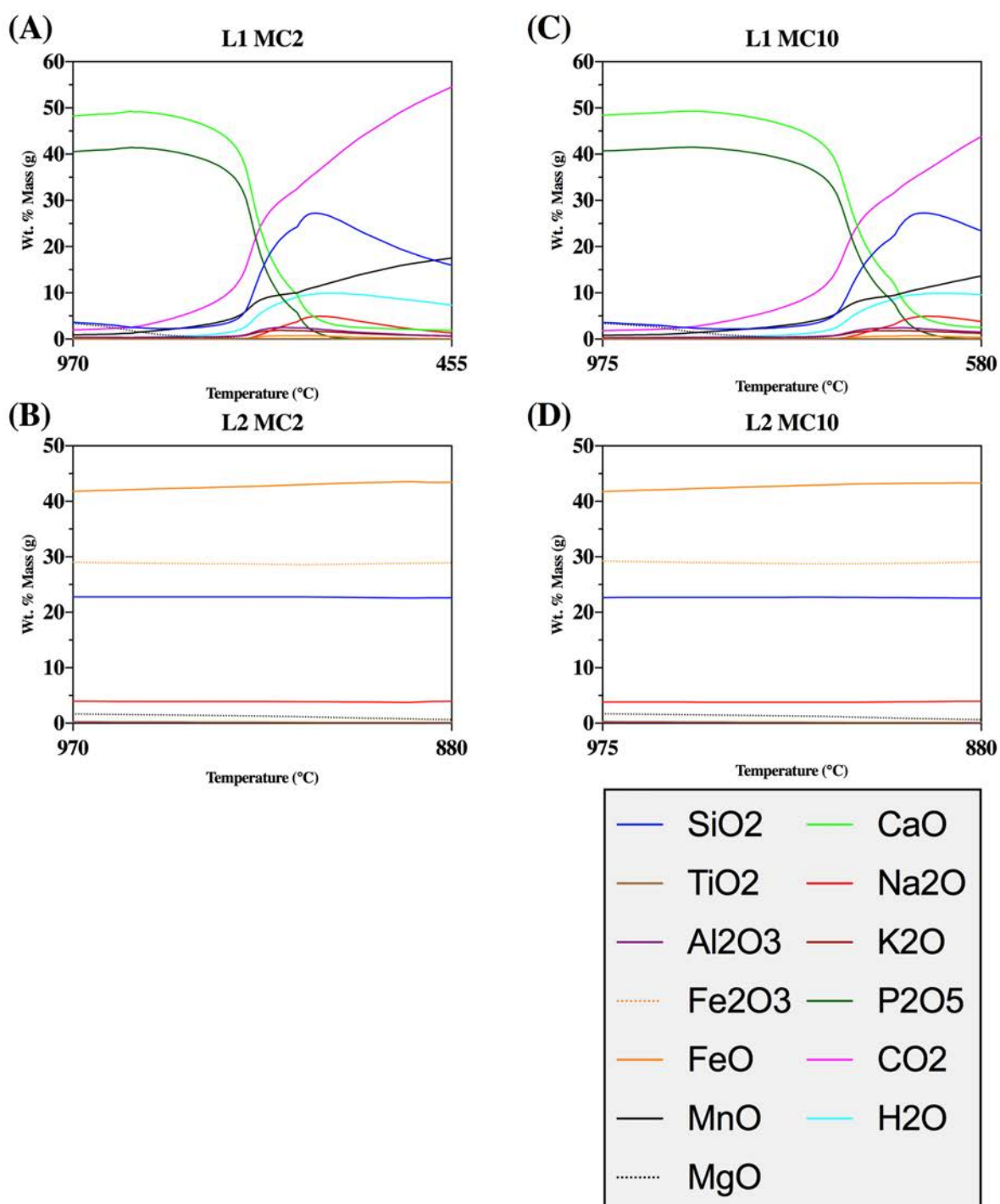


Figure 4.5: Each of the immiscible liquids to separate from the remaining liquids after adiabatic ascent. These liquids did not separate during ascent, but rather separated from the crystallization of the remaining liquid at the suggested emplacement pressure of 300 bars. (A) Liquid 1 from MC2. (B) Liquid 2 from MC2. (C) Liquid 1 from MC10. (D) Liquid 2 from MC10. In both data sets, Liquid 1 and Liquid 2 are nearly identical in composition between MC2 and MC10. The difference between all the separated liquids is the slight variation of the temperatures they separated from the initial magma at.

5 DISCUSSION

While the results obtained from alphaMELTS do not support Philpotts' (1972) hypothesis of liquid immiscibility, other data from the trials suggest consistency between alphaMELTS and observed minerals crystallized in the sill. Interpretations of the minerals calculated from alphaMELTS compared to published literature on the Ste. Dorothée Sill show similar modal mineralogy. One consideration in these interpretations is the accuracy of the alphaMELTS program for immiscible liquids. Despite the inconsistencies between Philpotts (1972) research and my alphaMELTS trials, other immiscible liquids produced may correlate to other tectono-magmatic processes in the Oka Pluton, another intrusion within the Montereignian Igneous Province. Further research on this topic will be needed to fully interpret and guarantee the accuracy of Philpotts (1972) hypothesis on the origin of the ocelli in the sill, but the results still provide data that suggests other important petrological interpretations.

5.1 Liquid Immiscibility in Alkaline Magmas

Liquid immiscibility has been shown to exist mainly in three types of magmas, with more research conducted on iron-rich tholeiitic magmas. Sulfide-saturated silicate magmas and highly alkaline magmas rich in CO_2 are widely accepted as the other two systems that exhibit liquid immiscibility (Winter, 2010). However, the magma emplaced to form the Ste. Dorothée Sill focused on in this thesis does not fall into these categories. Instead, the sill can be classified as an alkalic, silica-undersaturated intrusion with relatively low concentration of CO_2 . Philpotts (1972), the lead researcher on the study of the Ste. Dorothée Sill even suggests that liquid immiscibility is highly rare in alkaline basalts (Philpotts and Ague, 2009). Given this information, it is possible that the ocelli in the sill did not exist as an immiscible liquid, but instead as a separate liquid from fractional crystallization from the host fourchite.

5.2 Effectiveness of alphaMELTS for Modeling Liquid Immiscibility

The separation of liquids within each of the MC2 and MC10 trials does not occur unless the ‘Multiple Liquids’ or ‘Fractionate Second Liquid’ functions are turned on. This can be interpreted a few different ways. Either liquid immiscibility does not occur in the parental magma for the Sté Dorothée Sill or alphaMELTS is not able to accurately produce the separated liquids physically observed in the Ste. Dorothée Sill. One suggestion from the programmers and researches that developed alphaMELTS is the careful use of the ‘Multiple Liquids’ and ‘Fractionate Second Liquid’ functions. Particular to the ‘Multiple Liquids’ functions, they suggest that “the solvi are not very well determined, and [sic] do not recommend serious use of this feature, but in some cases operation inside an unrecognized two-liquid field can lead to path-dependent non-unique equilibria. This option should not be used if trace element calculations are enabled.” (Antoshechina and Asimow, 2018). Given that no research papers regarding liquid immiscibility in alkaline magmas are used for the calibration of the program, it is not unlikely that the program cannot calculate the immiscible liquids according to Philpotts’ (1972) findings. However, the immiscible liquids calculated from the isentropic trials may highlight larger tectono-magmatic processes that exist within the Montereian Igneous Province. This significance will be discussed in a later section.

For the most part, the mineral assemblages discussed in the following sections provide evidence that alphaMELTS crystallizes minerals consistent with Philpotts’ (1972) and Goldie’s (1972) findings.

5.3 Isobaric Interpretations

Philpotts (1972) originally suggests the ocelli formed after the emplacement of the sill, implying that only isobaric trials were needed to test his hypothesis. In order to test his

hypothesis using the alphaMELTS program, a total chemical composition for the sill that included both the ocelli and the groundmass was needed. By using the images provided in Philpotts' (1972) research, I found that the sill contained roughly 8% ocelli by volume. My volume calculation is strictly based on the limited number of images provided and Philpotts' descriptions in his paper. I have no personal field research on the sill, due to the inaccessibility of the area Philpotts researched. Other research conducted by R. J. Goldie suggests a total ocelli composition of 2.2% by volume (Goldie, 1972). Irrespective of which volume calculation is more accurate, I accounted for this discrepancy by running various ocelli volume proportions through the alphaMELTS software.

Starting with 2% ocelli relative to the host fourchite and working up towards 50% composition of ocelli in the total melt, I was able to determine that isobaric trials with melt composition of 10% or more of ocelli did not indicate a significant variance in the minerals crystallized. There is significant variance in the mineral assemblages between MC2 and MC10 which I will discuss in a later section. For this reason, I focus on the MC2 and MC10 trials to compare results between Goldie's (1972) research and my own ocelli volume calculation.

5.3.1 Mineral Interpretations

The minerals that crystallize from the isobaric trials in MC2 and MC10 vary from the given minerals observed by Goldie (1972) and Philpotts (1972). Philpotts defines the ocelli and felsic units as an analcite syenite. Analcite syenite is characterized by alkali feldspar, nepheline, analcite, some quartz, and minor amounts of hornblende and pyroxene. The host fourchite is composed of titanite, magnetite, minor plagioclase and alkali feldspar. The alphaMELTS results do not match these minerals exactly. A clinopyroxene with a composition similar to titanite crystallized in both of the MC2 and MC10 trials. Biotite also crystallizes from both

MC2 and MC10 liquids, but is not mentioned in Philpotts (1972) or Goldie's (1972) descriptions of the sill.

The crystallization leucite in the MC10 trial is the most noticeable difference between the MC2 and MC10 trials. Leucite is not mentioned in either Philpotts' (1972) research or Goldie's (1972) mineral analysis of the sill. However, the way in which Sack and Ghiorso (1998) have defined and programmed alphaMELTS to calculate leucite in a crystallizing magma provides the reason for crystalline leucite in the results. The empirical formula calculated by alphaMELTS in the isobaric trials is shown as: $K_{0.00}NaAlSi_2O_{5.12}(OH)_{1.77}$, whereas the accepted chemical formula for leucite is $K(AlSi_2O_6)$ (Mindat.org, 2019a). Within leucite, there exist 24 cavities in the unit cell which may contain water molecules under certain conditions (Sack and Ghiorso, 1998). In isostructural analcite, two thirds of these cavities are occupied by sodium atoms with H_2O replacing potassium on the larger site. Due to the small amounts of potassium in the mineral assemblage, alphaMELTS defined the precipitate as leucite. Based on my interpretation of the chemical composition, it is more likely that analcite is the mineral to precipitate out and not leucite. If this interpretation is valid, alphaMELTS is providing accurate information on the mineral assemblage of the fourchite surrounding the ocelli.

Taking a sample of the sill, I tested the rock for magnetism and found that it is magnetic, confirming the presence of a magnetic mineral like Philpotts (1972) suggests. The isobaric trials do not produce a magnetic mineral from either the MC2 or MC10 trials. Instead, the results show that iron is used in the clinopyroxene and biotite in each of the trials. If this is the case, the calculated biotite may have used up the remaining iron left in the melt, not allowing for a magnetic mineral to precipitate out. Neither Philpotts (1972) or Goldie (1972) see the presence of biotite in the host fourchite or ocelli. Given this information, it is more likely that the presence

of water in the bulk composition allowed biotite to crystallize and use the iron in solution, rather than producing a magnetic mineral.

5.4 Isentropic Interpretation

In the isentropic trials, I attempt to simulate the process of adiabatic ascent of the magma before emplacement. These trials suggest a more accurate representation of the mineral assemblage that exists in the Ste. Dorothée sill. Philpotts (1972) suggests that the ocelli separate from the magma post-emplacement, meaning that no liquid immiscibility occurs as the magma rises from depth. In the MC2 and MC10 isentropic trials, even with the *Multiple Liquids* and *Fractionate Second Liquid* functions turned on, there is no liquid separation from the initial magma. Even though both Philpotts (1972) and Goldie (1972) suggest 1100°C as the emplacement temperature, I use values of 1000°C and 1 GPa for the starting temperature and pressure of the trials to simulate the conditions at the base of the crust.

The minerals that crystallize out during ascent to the emplacement depth in the alphaMELTS trials seem to align more accurately with minerals observed by Philpotts (1972) and Goldie (1972). Titanaugite still crystallizes from both of the MC2 and MC10 liquids. Philpotts (1972) suggests that the phenocrysts of titanaugite that are seen in the sill must have crystallized before emplacement, aligning with the findings from the isentropic model. Moreover, the isentropic trials also produce an iron-rich spinel. The empirical formula produced by alphaMELTS suggests that the spinel would be magnetite. While the calculated formula contains both titanium and aluminum, it is common for these elements to exist in magnetite as impurities (Mindat.org, 2019b). This is consistent with my observations of the magnetism in the sill's hand sample.

5.4.1 Remaining Liquid after Adiabatic Ascent

The remaining liquid from the parent magmas of MC2 and MC10 after the ascent from 1 GPa to 0.03 GPa, give bulk composition data that closely resembles the composition of ocelli from Philpotts' (1972) paper. Table 4.5 from the results is provided below for interpretation. The remaining liquid from the isentropic ascent to the suggested emplacement depth imply that the ocelli may not have been of immiscible origin. The remaining liquid composition compared to the bulk composition of the ocelli provided by Philpotts (1972) is very similar, except for some minor oxides. Magnesium, phosphorus, and manganese oxides differ in composition, but all have relatively low weight percent, which shouldn't affect the mineralogy as much.

If I assume the ocelli did not form from immiscible liquids and instead are represented by the remaining liquids from the isentropic ascent from 1 GPa, some of the structures within the

Oxides	MC2	MC10	Philpotts (1972)
<i>SiO₂</i>	51.6	51.8	51.6
<i>TiO₂</i>	0.68	0.68	1.91
<i>Al₂O₃</i>	19.0	19.3	20.8
<i>Fe₂O₃</i>	1.00	1.02	1.20
<i>FeO</i>	2.71	2.67	2.76
<i>MnO</i>	0.54	0.50	0.16
<i>MgO</i>	0.78	0.76	1.10
<i>CaO</i>	4.10	4.02	4.86
<i>Na₂O</i>	8.17	8.12	7.25
<i>K₂O</i>	3.38	3.45	3.54
<i>P₂O₅</i>	0.84	0.82	0.12
<i>CO₂</i>	1.39	1.31	0.67
<i>H₂O</i>	5.73	5.60	4.36

Philpotts (1972) column shows the bulk composition data for the ocelli and felsic units

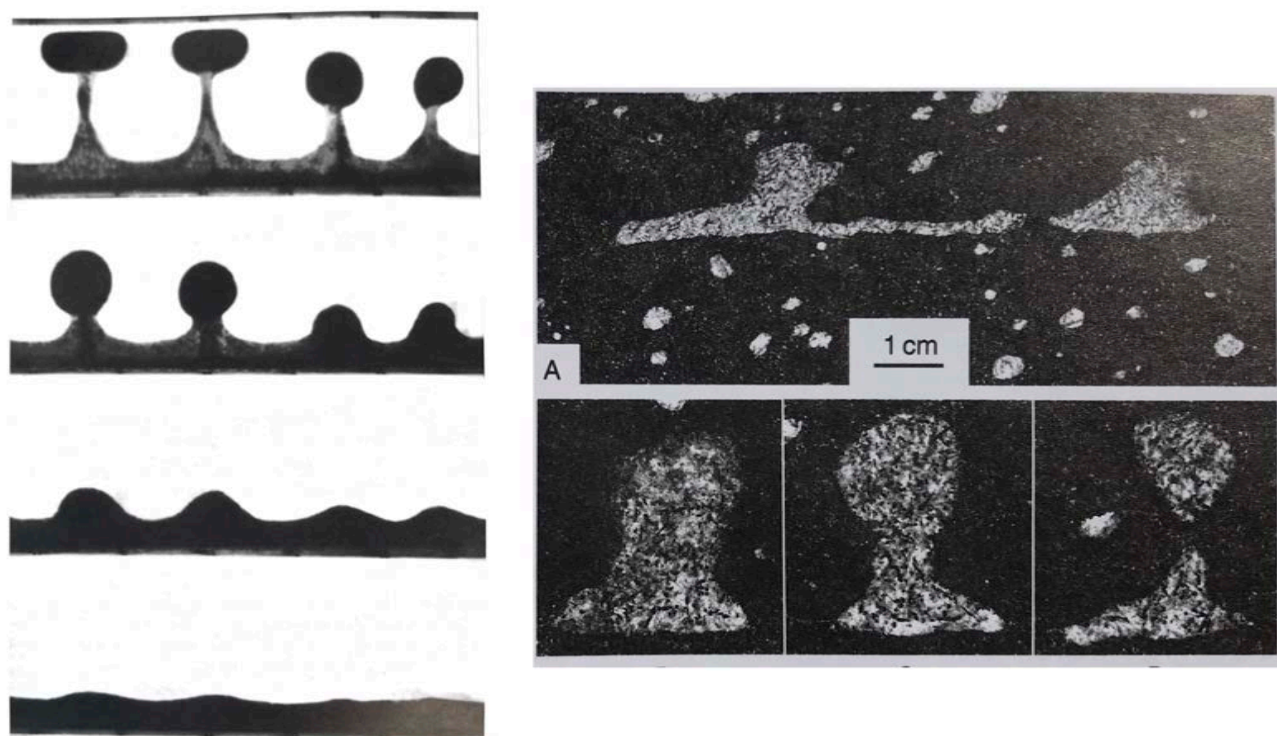


Figure 3.1: The image on the left shows an example of Rayleigh-Taylor instability. This shows the progressive stages of buoyantly rising domes of oil overlain with honey, which is of high density. Domes, such as the ones in the Sté Dorothée Sill are seen in the image on the right (Philpotts and Ague, 2009).

sill can be explained. If the remaining liquid intrudes as a separate layer either below or above the host fourchite magma, then diapiric structures would form based on Rayleigh-Taylor instability (Philpotts and Ague, 2009). Either the more dense, host fourchite would sink into the less-dense, felsic ocelli or vice versa. However, the smaller globular ocelli found at both the upper and lower contacts of the sill could not be explained by this phenomenon. It is still of interest that the remaining liquid from the isentropic ascent from 1 GPa produced a liquid that is chemically similar to that of Philpotts (1972) ocelli composition. If the remaining liquid is truly the source for the ocelli rather than immiscible origin, then the volume proportions of the ocelli would be different than the proposed ocelli volume of 2% from Goldie (1972) and my calculations of 10% by volume. In the MC2 and MC10 trials, 39 wt. % and 41 wt. % of the liquids remain by the time they reach 300 bars, respectively.

5.4.2 Crystallization of the Remaining Liquid After Adiabatic Ascent

After adiabatic ascent of the parent magma in both trials, there is 39 wt. % for MC2 and 41 wt. % in MC10 of liquids remaining by the time the melts reach 300 bars. Minerals that precipitate from the remaining melts are mostly consistent with the minerals observed by Philpotts and Goldie. The feldspar predicted to crystallize out from the alphaMELTS trials in both trials are rich in alkalis, similar to the actual groundmass of the sill. The crystallization of more alkali feldspars after the isentropic trials suggests similarities in published research. As the melt crystallizes during the ascent, the residual liquid becomes more felsic. This leaves more alkalis in the remaining liquid, causing alkali feldspar to precipitate out. The residual liquids also produce 34.1 wt. % of leucite in the MC2 and 26.2 wt. % in the MC10 trials, which coincides with Goldie's findings (Goldie, 1972).

The presence of alkalis has proven to expand the field of liquid immiscibility in tholeiitic magmas (Charlier and Grove, 2012; Freestone, 1978), so the separation of immiscible liquids during the isobaric crystallization of the remaining melt does not come as a surprise. As the melt crystallizes, the remaining liquid evolves to become more felsic, similar to a tholeiitic magma, allowing the opportunity for immiscible liquids to separate from the parent magma.

5.5 Significance of the Carbonate Liquids and the Oka Intrusion

The Oka pluton is a Cretaceous intrusive complex which is part of the broader Monteregian Hill igneous province. This pluton lies close to the Ste. Dorothee Sill and is relevant for the calcium rich immiscible liquids calculated from the alphaMELTS during the crystallization of the remaining liquids from the isentropic model. AlphaMELTS is largely based on research papers that focus on the evolution of tholeiitic magmas. Compositions that produce

calcium rich magmas won't necessarily produce results that mimic the mineralogy of the Oka pluton from the compositions calculated by the alphaMELTS program.

One of the most accepted mechanisms proposed for the formation of magmas rich in carbonatites is silicate-carbonate liquid immiscibility (Potter et al., 2017). Minerals produced from the remaining melt after the isentropic trials align well with the mineralogy of the Oka pluton. Allan Treiman and Eric Essene describe the pluton as an aggregate of carbonatite rocks, alnoite, and alkaline silicate rocks (Treiman and Essene, 1985).

A different rock type observed in the Oka pluton is a melteigite-urtite series. Urtite is a rock where the composition is dominated by nepheline and augite. Both nepheline and a titanite is calculated to precipitate from the remaining liquid in large proportions (Table 4.6).

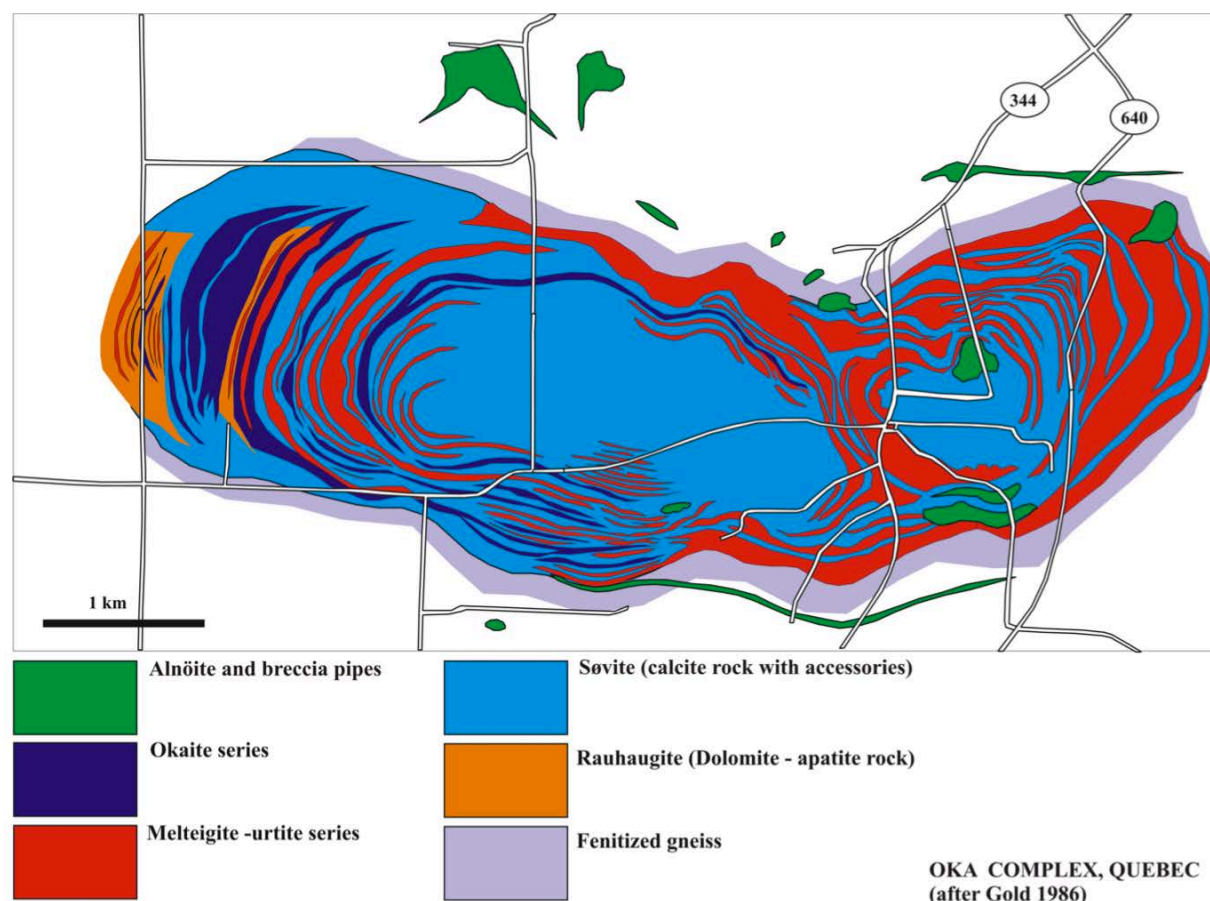


Figure 5.2: Simplified map of the Oka pluton. Cross-cutting dikes are seen represented by the white lines. (Lentz et al. 2006)

Seen in Figure 5.2, the Oka pluton is dominated by the Okaite series and the Melteigite-urite series. If I assume the remaining liquid over a larger scale represents the Oka pluton, then the remaining melt after the isentropic trials can be represented by this geologic feature. *

Further evidence for this assumption is also seen in the Okaite series. Okaite type rocks are dominated by silicates, usually melilite, nepheline, and hauyne (Potter et al., 2017). Potter equated the hauyne to an altered nepheline. If Potter's assumption is correct, then the okaite series is also represented by the mineralogy calculated from the remaining liquid.

Furthermore, the immiscible liquids from both the isobaric and isentropic models offer some similarities to the rock types found in the Oka Pluton. Liquid 1 from both the MC2 and MC10 isentropic trials and Liquid 1 from the isobaric trials have high proportions of calcium and phosphorous oxides initially, but as temperature decreases, these liquids become rich in CO_2 and SiO_2 . The interactions between these oxide groups might imply that calcite minerals will precipitate out, which correspond to the Sovite group seen in Figure 5.1. While the compositions of the liquids do not entirely match that of the Oka Pluton, it provides information that suggests carbonate magmas can separate immiscibly from alkalic magmas.

5.6 Future Work

In order to definitively defend Philpott's (1972) hypothesis or refute the possibility for liquid immiscibility in the Sté Dorothée Sill, viscosity measurements between the host fourchite and the ocelli would be needed. Viscosity measurements would be helpful in deciding if the remaining liquids, discussed in Section 5.4.1, would deform in the way they are seen in the sill. If the host fourchite is already crystallized, then the viscosity measurements would determine if this liquid could deform the partially crystallized fourchite. Recent studies have suggested that Rayleigh-Taylor instability is observed in partially crystallized magmas (Seropian et al., 2018).

Considering the remaining liquid composition after the isentropic ascent from 1 GPa, viscosity measurements at various points during crystallization of the host fourchite could determine if the diapiric structures observed in the sill are the result of this instability.

6 CONCLUSION

Liquid immiscibility is a common occurrence, mostly observed in thin section analysis of quenched magmas. However, large scale immiscible liquids are only hypothesized in many cases due to the complete separation from their respective parental magmas. Viewing such large scale processes become difficult as the separation of these liquids occur either deep in the crust or in the mantle. The immiscible liquids hypothesized by Philpotts (1972) in the Sté Dorothée Sill offer potential evidence for small scale immiscible structures within a small intrusion.

Results from this research suggest that the ocelli seen in the Sté Dorothée sill are not of immiscible origin. Any immiscible liquids to separate out from either the isobaric or isentropic trials did not match that of Philpotts (1972) or Goldie's (1972) chemical compositions. The immiscible liquids calculated using alphaMELTS in both the isobaric and isentropic models can be described as iron-rich silicate liquids, calcium phosphates, or carbonate liquids. Despite the lack of evidence to support the immiscible liquid hypothesis, I was able to produce a mineralogical composition from the alphaMELTS program that is similar to the minerals found within the Sté Dorothée Sill.

One major caveat in this thesis is the lack of published research on liquid immiscibility in alkaline magmas. Extensive research has been conducted on liquid immiscibility in tholeiitic magmas (Charlier and Grove, 2012) and is currently the only accepted hypothesis for the differentiation of carbonate magmas (Potter et al., 2017; Treiman and Essene, 1985). Few researchers have been able to definitely prove liquid immiscibility in alkaline magmas.

The remaining liquids after adiabatic ascent in the isentropic model suggest a different origin for the ocelli in the Sté Dorothée Sill. The bulk composition data from the remaining liquid has stark similarity to Philpotts (1972) bulk compositions data of the ocelli. Given that the

isentropic model is an attempt to replicate realistic conditions of emplacement, it is likely that the ocelli did not originate from immiscible origin. Rather, the ocelli may have been the result of fractional crystallization as the entire parental magma ascended from depth. More research is needed to strengthen this hypothesis because it cannot accurately describe all of the ocelli structures seen in the sill.

REFERENCES

- Allègre, C. J., Dupré, B., Lambret, B., and Richard, P., 1981, The subcontinental versus suboceanic debate, I Lead-neodymium-strontium isotopes in primary alkali basalts from a shield area the Ahaggar volcanic suite: *Earth and Planetary Science Letters* v. 52, no. 1, p. 85-92.
- Antoshechina, P., and Asimow, P., 2018, alphaMELTS Software Manual, A text driven interface for MELTS, pMELTS, and pHMELTS: California Institute of Technology, California Institute of Technology.
- Antoshechkina, P., Ghiorso, M., and Asimow, P., 2012, alpaMELTS, Caltech.
- Bowen, N. L., 1928, Liquid Immiscibility in Silicate Magmas, *The Evolution of the Igneous Rocks*: Princeton, New Jersey, Princeton University Press, p. 7-19.
- Charlier, B., and Grove, T. L., 2012, Experiments on liquid immiscibility along tholeiitic liquid lines of descent *Contributions to Mineralogy and Petrology*, v. 164, p. 27-44.
- Clark, T. H., 1972, *Region de Montreal Area*: Ministère Des Richesses Naturelles, v. 152.
- Crough, S. T., 1981, Mesozoic hotspot epeirogeny in eastern North America *Geology*, v. 9, p. 2-6.
- Eby, G. N. and McHone, J. G., 1997, Plutonic and hypabyssal intrusions of the Early Cretaceous Cuttingsville Complex, Vermont. In Grover, T. W., Mango, H. N. and Hasenohr, E. J. (eds.) *Guidebook to Field Trips in Vermont and Adjacent New Hampshire and New York*. New England Intercollegiate Geological Conference, Castleton, VT, pp. B2-1 - B2-17.
- Eby, N., 1985, Sr and Pb isotopes, U and Th chemistry of alkaline Montereian and white Mountain igneous provinces, eastern North America.: *Geochimica et Cosmochimica Acta*, v. 49, no. 5, p. 1143-1153.
- Freestone, I. C., 1978, Liquid immiscibility in alkali-rich magmas: *Chemical Geology*, v. 23, no. 1, p. 115-123.
- Goldie, R. J., 1972, *Petrology and Geochemistry of a Montereian Sill near Ste. Dorotheé*, Quebec [Master of Sciences: McGill University].

Haase, K. M., and Renno, A. D., 2008, Variation of magma generation and mantle sources during continental rifting observed in Cenozoic lavas from the Eger Rift, Central Europe: *Chemical Geology*, v. 257, no. 3-4, p. 192-202.

HMXEarthScience, Continental Crust:

<https://hmxeearthscience.com/Sammartano/DYNAMIC%20CRUST%2013/Earth%27s%20Interior%20STUDENT.key/Data/>.

Howard, W. V., F. D. Adams, and H. Cooke, 1922, Some Outlines of the Monteregian Hills. *Trans. Roy. Soc. Canada*, 3rd ser., 16, sec. 4, p. 47-95.

Irvine, T. N., and Baragar, W. R. A., 1971, A Guide to the Chemical Classification of the Common Volcanic Rocks: *Canadian Journal of Earth Sciences*, v. 8, p. 523-548.

Kieffer, S. W., and Delany, J. M., 1979, Isentropic decompression of fluids from crustal and mantle pressures: *Journal of Geophysical Research*, v. 84, no. B4, p. 1611-1620.

Lentz, D., Eby, N., Park, A., and Lavoie, S., 2006, Diatremes, dikes, and diapirs: Revisiting ultra-alkaline to carbonatitic magmatism of the Monteregian Hills. Geological Association of Canada - Mineralogical Association of Canada, Joint Annual Meeting, Montreal 2006, Field Trip B4 Guidebook, 49 p.

McHone, J. G., 1996, Constraints on the Mantle Plume model for Mesozoic Alkaline Intrusions in Northeastern North America: *Canadian Minerologist*, v. 34, p. 325-334

Mindat.org, 2019a, Leucite, Hudson Institute of Mineralogy.

-, 2019b, Magnetite, Hudson Institute of Mineralogy.

Mitchell, R. H., 1996, Classification of Undersaturated and Related Alkaline Rocks, Winnipeg, Manitoba, Mineralogical Association of Canada, Undersaturated Alkaline Rocks: Mineralogy, Petrogenesis, and Economic Potential.

Philpotts, A. R., 1972, Density, surface tension and viscosity of the immiscible phase in a basic, alkaline magma: *Lithos*, v. 5, no. 1, p. 1-18.

Philpotts, A. R., 1982, Compositions of Immiscible Liquids in Volcanic Rocks: Contributions to Mineralogy and Petrology, v. 80, no. 3, p. 201-218.

Philpotts, A. R., and Ague, J. J., 2009, Principles of Igneous Metamorphic Petrology, Cambridge, United Kingdom, Cambridge University Press, 667 p.:

- Philpotts, A. R., and Hodgson, C. J., 1968, Role of Liquid immiscibility in Alkaline Rock Genesis, *in* Kuthan, M., Fiala, F., Konocny, V., and Shrbeny, O., eds., International Geological Congress, Volume 2: Prague, Czechoslovakia, p. 175-188.
- Potter, N. J., Kamenetsky, V. S., Simonetti, A., and Geomann, K., 2017, Different types of liquid immiscibility in carbonatite magmas: A case study of the Oldoinyo Lengai 1993 lava and melt inclusions: *Chemical Geology*, v. 445, p. 376-384.
- Roedder, E., 1951, Low temperature liquid immiscibility in the system $K_2O-FeO-Al_2O_3-SiO_2$: *American Mineralogist*, v. 36, no. 3-4, p. 282-286.
- Sack, R. O., and Ghiorso, M. S., 1998, Thermodynamics of feldspathoid solutions: Contributions to Mineralogy and Petrology, v. 130, no. 3-4, p. 256-274.
- Sengör, A. M. C., and Burke, K., 1978, Relative timing of rifting and volcanism on Earth and its tectonic implications: *Geophysical Research Letters*, v. 5, no. 6, p. 419-421.
- Seropian, G., Rust, A. C., and Sparks, R. S. J., 2018, The Gravitational Stability of Lenses in Magma Mushes: Confined Rayleigh-Taylor Instabilities: *Journal of Geophysical Research: Solid Earth*, v. 123, no. 5, p. 3593-3607.
- Treiman, A. H., and Essene, E. J., 1985, The Oka carbonatite complex, Quebec: geology and evidence for silicate-carbonatite liquid immiscibility *American Mineralogist*, v. 70, p. 1101-1113.
- Visser, W., and Groos, K. V., 1979, Effects of P_2O_5 and TiO_2 on liquid-liquid equilibria in the system $K_2O-FeO-Al_2O_3-SiO_2$: *American Journal of Science*, v. 279, no. 8, p. 970-988.
- Winter, J. D., 2010, *An introduction to igneous and metamorphic petrology*, Upper Saddle River, New Jersey, Pearson Prentice Hall, 702 p.:

APPENDIX A: EQUATIONS

Figure 1.1: Equation governing the line that defines the boundary between the subalkaline series and the alkaline series.

$$\begin{aligned} SiO_2 = & -3.3539 \times 10^{-4} \times A^6 + 1.2030 \times 10^{-2} \times A^5 \\ & -1.5188 \times 10^{-1} \times A^4 + 8.6096 \times 10^{-1} \times A^3 \\ & -2.1111 \times A^2 + 3.9492 \times A + 39.0 \end{aligned}$$

Figure 1.3: Equation governing the distinction between alkaline and subalkaline rocks on a ternary plot.

$$Ne' = Ne + \frac{3}{5}Ab, Q' = Q + \frac{2}{5}Ab + \frac{1}{4}Opx, \text{ and } Ol' = Ol + \frac{3}{4}Opx$$

Figure 1.5: (Irvine and Baragar, 1971)

Symbols used:

Ol = olivine, cation norm

An = Anorthite

Ab = Albite

CI = Color Index $P = 100 An/(An + Ab)$, cation norm

Fig. 1.5 A Classification of the sodic alkali olivine basalt series.
Examined on the following sequence of tests, the rock is:

- (a) picrite basalt if $Ol \geq 25\%$
- (b) ankaramite if $CI \geq 30 + \frac{5}{6}(80 - P)$
- (c) nephelinite if $CI \geq 30 + \frac{5}{9}P$
- (d) alkali basalt if $CI \geq 80 - P$
- (e) hawaiite if $CI \geq 50 - P$
- (f) mugearite if $CI \geq 30 - P$
- (g) benmorite if $CI \geq 20 - P$
- (h) sodic trachyte if $CI < 20 - P$

Fig. 1.5 B Classification of the potassic alkali olivine basalt series.
Examined in the following sequence of tests, the rock is:

- (a) picrite basalt if $Ol \geq 25\%$
- (b) ankaramite if $CI \geq 20 + \frac{5}{6}(80 - P)$
- (c) alkali basalt if $CI \geq 70 - P$
- (d) trachybasalt if $CI \geq 40 - P$
- (e) tristanite if $CI \geq 20 - P$
- (f) trachyte if $CI < 20 - P$

(Irvine and Baragar, 1971)

Section 1.7 Stokes Law

Stokes Law used for the velocity measurements of the ocelli within the fourchite.

$$\frac{dx}{dt} = \frac{2g\Delta\rho r^2}{9\eta}$$

APPENDIX B: MELTS FILES

Environment File for alphaMELTS. The highlighted areas indicate the functions that are turned on and off during the data analysis. Exclamation marks indicate that the function is turned on.

```
!Default values of environment variables (version 1.6)
!Variables preceded by '!' are 'unset' (i.e. 'false')
```

```
ALPHAMELTS_VERSION MELTS
!ALPHAMELTS_OLD_GARNET true
!ALPHAMELTS_OLD_SPINEL true
!ALPHAMELTS_OLD_BIOTITE true
!ALPHAMELTS_2_AMPH true
!ALPHAMELTS_NO_CHLORITE true
ALPHAMELTS_MODE isobaric
!ALPHAMELTS_PTPATH_FILE filename
ALPHAMELTS_DELTAP +0
ALPHAMELTS_DELTAT -5
ALPHAMELTS_MAXP +300
ALPHAMELTS_MINP +300
ALPHAMELTS_MAXT +1900
ALPHAMELTS_MINT +800
!ALPHAMELTS_ALTERNATIVE_FO2 true
!ALPHAMELTS_LIQUID_FO2 true
!ALPHAMELTS_IMPOSE_FO2 true
!ALPHAMELTS_FO2_PRESSURE_TERM true
!ALPHAMELTS_CONTINUOUS_MELTING true
ALPHAMELTS_MINF 0.005
!ALPHAMELTS_MINPHI 0.002
!ALPHAMELTS_CONTINUOUS_RATIO float
!ALPHAMELTS_CONTINUOUS_VOLUME true
!ALPHAMELTS_FRACTIONATE_SOLIDS true
ALPHAMELTS_MASSIN 0.001
!ALPHAMELTS_FRACTIONATE_WATER true
!ALPHAMELTS_MINW float
!ALPHAMELTS_FRACTIONATE_TARGET true
!ALPHAMELTS_MGO_TARGET 8.0
!ALPHAMELTS_MGNUMBER_TARGET float
!ALPHAMELTS_ASSIMILATE true
!ALPHAMELTS_FLUX_MELTING true
!ALPHAMELTS_DRY_ITER_PATIENCE 100
!ALPHAMELTS_D0_TRACE true
!ALPHAMELTS_D0_TRACE_H2O true
!ALPHAMELTS_HK_OL_TRACE_H2O true
!ALPHAMELTS_HK_PXGT_TRACE_H2O true
!ALPHAMELTS_2X_OPX_TRACE_H2O true
!ALPHAMELTS_TRACE_DEFAULT_DPTX true
!ALPHAMELTS_TRACE_NORMALIZATION integer
!ALPHAMELTS_TRACE_INPUT_FILE filename
!ALPHAMELTS_TRACE_USELIQFEMG true
!ALPHAMELTS_MULTIPLE_LIQUIDS true
!ALPHAMELTS_FRACTIONATE_SECOND_LIQUID true
!ALPHAMELTS_FOCUS true
!ALPHAMELTS_FOCUS_FACTOR float
!ALPHAMELTS_ADIABAT_FILE true
!ALPHAMELTS_CELSIUS_OUTPUT true
!ALPHAMELTS_SAVE_ALL true
!ALPHAMELTS_SKIP_FAILURE true
!ALPHAMELTS_FAILED_ITER_PATIENCE 10
!ALPHAMELTS_INTEGRATE_FILE filename
!ALPHAMELTS_LATENT_HEAT true
!ALPHAMELTS_QUICK_OUTPUT true
```